Physics – Uspekhi **62** (9) 865 – 891 (2019)

REVIEWS OF TOPICAL PROBLEMS PACS numbers: 71.35.Lk, 73.21.Fg, 78.67.De

Spin excitations in two-dimensional electron gas, their relaxation, photoexcitation, and detection methods, and the role of Coulomb correlations

L V Kulik, A V Gorbunov, S M Dickmann, V B Timofeev

DOI: https://doi.org/10.3367/UFNe.2018.10.038463

Contents

Abstract. **We discuss spin excitations in a degenerate 2D electron gas in a perpendicular quantizing magnetic field: spin-wave and 'Goldstone' excitons in a quantum Hall ferromagnetic (filling factor $\nu = 1$), and spin-cyclotron excitons in a quantum Hall insulator ($\nu = 2$). The latter exhibit record-setting long lifetimes, up to 1 ms, owing to which a transition to a basically new collective state, a magnetofermionic condensate, is observable at temperatures $T < 1$ K. The condensate's properties may be explained in terms of a coherent state being formed due to the emergence of a dense ensemble of photoexcited long-lived spin-cyclotron excitons obeying Bose statistics in a nonequilibrium system of 2D fermions.**

Keywords: magnetoexcitons, quantum Hall insulator, quantum Hall ferromagnet, collective excitations, magnetofermionic condensate

1. Introduction

Almost all recent innovative achievements in solid state technologies are based in one way or another on the creation of new materials and material systems (quasi-two-dimensional, quasi-one-dimensional, and quasi-zero dimensional heterostructures, layered structures, carbon low-dimensional systems, etc.) or the development of new physical approaches to seemingly known phenomena (superconducting and semiconductor qubits, single-photon radiation sources, quantum cryptography, etc.).

A great amount of recent attention of researchers has been devoted to spintronics — the field of technological applications involving the manipulation of the spin degree of freedom [1]. Magnonics based on using spin waves (magnons) for manipulations and transfer of signals has also been developed [2]. Even more exotic applications assume the involvement of vortex spin excitations, skyrmions, in spin dynamics. Experimental studies on the control of skyrmions and measurements of their mass and mean free path have appeared [3]. It is expected that nondissipative spin transport can be achieved in a system of skyrmions.

The study of spin-dependent phenomena in two-dimensional electron systems (2D ESs) is attracting great interest due to the widening possibility of developing new devices for manipulating electron spins. An electron can be in two spin states, which is very convenient for coding data bits. The control of electron spin states can be used in the future to create high-speed logic gates and memory arrays with low energy consumption and great information capacity.

One of the most interesting ideas of spintronics is the creation of a spin transistor based on the control of the spin precession of charge carriers by an external electric field using the modulation of the spin-orbit interaction energy by a gate voltage [4]. The fundamental possibility of controlling the spin polarization by an electric field could make an invaluable contribution to the development of spintronics. However, this

L V Kulik [(1)], **A V Gorbunov** [(2)], **S M Dickmann** [(3)], **V B Timofeev** [(4)]
Institute of Solid State Physics, Russian Academy of Sciences,
ul. Akademika Osip'yana 2, 142432 Chernogolovka, Moscow region, Russian Federation
E-mail: [(1)] kulik@issp.ac.ru, [(2)] gorbunov@issp.ac.ru,
[(3)] dickmann@mail.ru, [(4)] timofeev@issp.ac.ru

Received 15 June 2018, revised 11 October 2018
Uspekhi Fizicheskikh Nauk **189** (9) 925 – 954 (2019)
DOI: https://doi.org/10.3367/UFNr.2018.10.038463
Translated by M Sapozhnikov; edited by V L Derbov

beautiful idea has not been fully realized in practice so far, despite its attractiveness, in particular because of problems related to the fast relaxation of spin excitations.

Single-particle spin relaxation channels are determined by the presence or absence of inversion symmetry in an electron system. For symmetric systems, the main one is the Elliot–Yafet relaxation mechanism, and for nonsymmetric systems it is the D'yakonov–Perel' mechanism. These two relaxation mechanisms were recently combined within the framework of a unified theory in papers [5, 6], which gives grounds to expect the appearance of a more general theory considering a quantizing magnetic field and many-particle Coulomb interaction. A reduction in the system's dimensionality (quantum confinement) and a quantizing magnetic field substantially reconstruct a single-particle energy spectrum, making it effectively zero-dimensional. In this case, standard single-particle relaxation mechanisms are suppressed, resulting in an increase in the spin relaxation time. Simultaneously, new mechanisms arise which, in turn, reduce the spin relaxation time. For example, spatial fluctuations of the external electrostatic potential not only lift the degeneracy of Landau levels but also cause weak and smooth spatial fluctuations of the g-factor. The latter, however, can be sufficient to produce a dephasing of coherent spin precession with respect to the magnetic field, because electron spins at different spatial points precess at different rates.

Fundamentally new spin relaxation channels appear when the Coulomb interaction between particles is taken into account. Although the transport, optical, and magnetic phenomena in strongly correlated 2D ESs have been well studied, so far no definite physical model of spin relaxation in quantizing magnetic fields has been developed, which is explained by a great number of competing spin relaxation mechanisms and the difficulty of describing the influence of the Coulomb interaction on relaxation mechanisms. On the one hand, two-dimensionality substantially increases the spin-orbit interaction for conduction electrons in $GaAs/Al_xGa_{1-x}As$ heterostructures.[1] On the other hand, Coulomb correlations dramatically reconstruct the energy spectrum, which can result in deceleration of the spin relaxation rather than its acceleration. Spin relaxation times measured by indirect transport and optical methods vary in a very broad range [7–10], which complicates the choice of a certain relaxation mechanism for explaining the experimental data available.

Nevertheless, this question has been attracting theoretical interest for a long time (see, for example, paper [11], in which Coulomb correlations were disregarded). Later, the spin relaxation was theoretically investigated mainly in a quantum Hall ferromagnet [12–14] formed after the filling by electrons of one Landau spin sublevel (the electron filling factor $\nu = 1, 3, \ldots$) and recently in a quantum Hall insulator [15] formed upon the complete filling of Landau levels by electrons ($\nu = 2, 4, \ldots$).

A quantum Hall ferromagnet is, in fact, a test system for studying the influence of the Coulomb interaction (both direct and exchange) on the spin excitation spectrum, because the agreement between experimental data and theoretical calculations describing the spectrum of excited states proves to be so close that it is often within the experimental error [16]. In this case, the multiparticle Coulomb interaction is included in the theory directly *ab initio* without using any models (applied in the theory of usual 'classical' magnetics). Therefore, for example, the study of a nonequilibrium spin system in a quantum Hall ferromagnetic is the most direct method for estimating the influence of multiparticle Coulomb correlations on the spin relaxation in 2D ESs.

The main theoretical approach for solving problems discussed in this review is the exciton representation (ER) method. The idea, which was proposed by L V Keldysh back in the 1960s [17–20], consists of passing from the single-particle basis set of states of the ideal gas to the basis of single-exciton states created by the action of exciton operators on a conditional vacuum (i.e., the ground state). This transformation is sometimes called bosonization, because the exciton gas actually obeys the Bose statistics. At the same time, exciton operators themselves are neither bosonic nor fermionic. They represent a sum of two operators, each of them, in turn, being a product of the electron and hole Dirac creation operators.

In due time, the idea of the exciton basis applied to problems related to classical semiconductors was not developed for a number of reasons, whose explanation is irrelevant here. However, this idea was revived in the 1980s, when the study of two-dimensional electron-hole ensembles in strong magnetic fields began to attract interest [21, 22]. An exciton operator applied to quantum Hall systems represents a certain 'correct' combination of the products of the electron annihilation operator in a state below the Fermi level and the electron creation operator in a state above the Fermi level.

The basis states of the ER are magnetoexcitons, which were considered for the first time for a 3D space by L P Gor'kov and I I Dzyaloshinskii [23]. Magnetoexcitons in a quantum Hall system are excitations in the conduction band formed by an electron vacancy at the lower Landau level, i.e., below the Fermi level (hereafter for brevity, a Fermi hole), and an electron in some other state (orbital or spin) with a higher energy. While in the basis of single-particle states only the single-particle part of the system Hamiltonian is diagonal, in the basis of exciton states a considerable part of the Coulomb interaction Hamiltonian is also diagonalized.

In a certain sense, the exciton representation for the Coulomb interaction is a 'correct' basis set for zero-order approximation. In particular, exciton basis states are classified by a natural quantum number, the wave vector of a magnetoexciton, i.e., an invariant appearing because of the translation symmetry of the system in a homogeneous magnetic field [23]. The degeneracy of the basis proves to be lifted to a considerable degree (only the degeneracy over the wave-vector directions remains).

The exciton representation has a number of other obvious advantages. It is independent of the particular calibration of single-electron wave functions in a magnetic field. The four-operator Coulomb interaction Hamiltonian transforms into the two-operator expression. This representation gives eigenstates in the explicit form, allowing us to calculate the matrix elements of transitions with the help of some quite definite commutative Lie algebra for exciton operators, thereby finding the probabilities of various kinetic processes in an electron (exciton) gas.[2] Finally, exciton states or their combinations in many important cases are asymptotically exact eigenstates of the Hamiltonian of a

[1] $GaAs/Al_xGa_{1-x}As$ structures are the most interesting for verifying the spin relaxation theory in strongly correlated high-mobility 2D systems.

[2] These transitions may be related, for example, to the 'interexciton' interaction due to the presence of 'exciton-nondiagonalized' terms in the Coulomb Hamiltonian and to the electron–phonon, electron–impurity, and other interactions, which are renormalized, respectively, to exciton–exciton, exciton–phonon, exciton–impurity, etc. interactions.

quantum Hall system in the first approximation with respect to the Coulomb interaction.

Note that the commutation algebra of exciton operators is not related to bosons, which can be associated with the appearance of some 'kinematic' interaction between excitons not related to the Coulomb (i.e., dynamic) interaction, but explained, of course, by the Fermi nature of an electron and a hole forming a magnetoexciton [24]. In a 'diluted' gas of magnetoexcitons, whose number is much smaller than the number of states at the Landau level, we can ignore in the zeroth-order approximation both kinematic and dynamic interactions, but consider them perturbative in problems related, for example, to the scattering of magetoexcitons by each other or in external fields (by phonons or a random electrostatic potential existing in a quantum well [see, for example, Section 3 and references therein]).

At the same time, problems concerning calculations of the magnetoexciton energy determined by the Coulomb interaction require, of course, the use of exact commutation relations for exciton operators. This makes it possible to calculate in some important cases the excitation energy in such a strongly correlated multiparticle system, which is determined even by the second-order Coulomb interaction (see Section 5 and references therein). The exact commutation algebra is also used in studies of a magnetoexciton condensate, i.e., when a macroscopically large number of excitations are in the same state with the same wave vector. Such calculations were first performed for a condensate in a conditional symmetric two-component electron-hole system [25]. Magnetoexciton condensates are considered in Sections 6 and 8.

In the theory of a quantum Hall ferromagnet ($\nu = 1$), as in the case of a usual exchange ferromagnet described, for example, by the Heisenberg Hamiltonian, the deviation of a spin system from equilibrium can be microscopically represented as the appearance of spin excitations. These excitations are, for example, spin waves (Bloch magnons in an exchange ferromagnet [26]) reducing by unity the total spin S of the system and the component S_z directed along the magnetization axis. At the same time, if the wave vector of a spin wave/magnon is strictly zero, such an excitation becomes qualitatively different, still changing the component S_z by unity, but preserving the total spin. This property is common to magnets of all types and is independent of the method used to describe the interaction: either with the help of the total Coulomb Hamiltonian or by a model with the Heisenberg operator. The spin-wave creation operator for the wave vector $k \equiv 0$ is equivalent simply to the total operator $S_- = S_x - \mathrm{i}S_y$ [26], while the excitation itself causes the transition to the eigenstate of the system with the previous orbital wave function but with the spin globally deviated from the magnetization axis, because now $S > S_z$.

The simplest excitation in a quantum Hall ferromagnet ($\nu = 1$) consists of a Fermi hole at the filled lower spin sublevel of the zero Landau level and an electron with the opposite spin excited up to the unfilled upper spin sublevel of the same Landau level. This is just the case corresponding to spin-wave excitation, i.e., for the nonzero wave vector, both the total spin of the electron system and its projection on the magnetic field direction decrease by unity.

The appearance of a spin wave with a strictly zero momentum similarly changes the spin projection on the magnetic field direction but preserves the total spin of the electron system. Such a 'zero' spin magnetoexciton corresponds to elementary excitation describing the global deviation of the total spin of the electron system from the magnetic field direction by some angle. For a macroscopically large number of excited 'zero' spin magnetoexcitons or even for a superposition of states with different numbers of 'zero' magnetoexcitons, the orbital state of a quantum Hall system does not change. However, the macroscopic state represents a Goldstone mode — the deviation of the total spin by some angle from the direction $\hat{z}$ (see [13] and the beginning of Section 4).

We will call 'zero' spin magnetoexcitons Goldstone excitons (X_G) and denote spin-wave excitons by $X_{\mathbf{q}}$. The spin relaxation process in both cases can be described in terms of annihilation of spin magnetoexcitons. In experiments related to the creation of nonequilibrium systems using optical methods, a situation is realized in which the total spin of the electron system is always directed along the magnetic field, but its value differs from the spin of the equilibrium system. In this case, the number of Goldstone excitons is, obviously, negligibly small compared to the total number of spin (in fact, 'nonzero' spin-wave) magnetoexcitons in the system.

The relaxation or annihilation process of spin-wave magnetoexcitons is determined by the Rashba and Dresselhaus spin-orbit interactions. In addition, these processes highly depend on a long-wavelength random potential, which is always present in 2D systems. Therefore, studies of relaxation problems for localized and delocalized spins should be separated.

Theoretical estimates of the relaxation time of spin excitations in a quantum Hall ferromagnet vary from a few hundred nanoseconds to a few tens of microseconds. In addition, these estimates were not consistent with indirect experimental data giving relaxation times not exceeding 10 ns. Such a drastic discrepancy between theory and experiment can be explained by the fact that spin relaxation times were not directly measured in experiments where only the dephasing time of the spin precession was estimated, which can be considerably shorter than the energy relaxation time related to the change in the Zeeman energy.

Electron excitations in the theory of a quantum Hall insulator ($\nu = 2$) are magnetoexcitons formed by an excited electron at the first unfilled Landau level and a Fermi hole (electron vacancy) at the completely filled zero Landau level. The excitation spectrum of a quantum Hall insulator contains two types of magnetoexcitons: a spin-singlet magnetoexciton with zero total spin and a cyclotron spin-triplet magnetoexciton with a total spin of unity. A spin-singlet magnetoexciton is nothing but a magnetoplasmon (spinless excitation) with energy at the zero wave vector equal to the single-particle cyclotron energy, according to the Kohn theorem [27, 28].

At the same time, the components of a triplet spin exciton (for which $S = 1$ and $S_z = -1, 0, +1$) are separated from each other by the Zeeman gap. Note that for the zero wave vector ($q = 0$) and even for other actual values $q \lesssim 1/l_B$ (where $l_B = \sqrt{\hbar c/eB}$ is the magnetic length), the entire triplet in $GaAs/Al_xGa_{1-x}As$ proves to be lower than the unfilled Landau level, i.e., its energy is smaller than the cyclotron gap by some additional 'coupling energy' determined by Coulomb correlations in 2D ESs [29–31].

The negative 'Coulomb shift' allows one to assume that the component of such a spin-cyclotron exciton corresponding to $S_z = +1$ is the lowest-energy[3] excitation for $\nu = 2$.

[3] This is a component with the positive projection S_z on the magnetic field direction (which we assume to be positive), because the electron g-factor in GaAs is negative.

Unlike a magnetoplasmon, a spin-cyclotron exciton is optically inactive. It represents the so-called dark exciton because its radiative recombination is spin-forbidden. Nevertheless, using resonance interband transitions, namely, dipole-allowed optical transitions between the discrete states of heavy holes in the valence band (corresponding to Landau levels with numbers $n_L > 1$) and electron states in the conduction band, it is possible to create a nonequilibrium ensemble of such magnetoexcitons [32].

The change in the spin in 2D ESs is mainly caused by the spin flip of a photoexcited hole due to a strong spin-orbit interaction in the valence band of GaAs. During the subsequent transformation of the photoexcited heavy hole from the valence band to a Fermi hole of the electron system, which occurs due to recombination of electrons from the zero filled Landau level with the photoexcited hole of the valence band, the electron system changes its spin. Since the direct relaxation of spin-cyclotron excitons to the ground state followed by the simultaneous change in orbital and spin quantum numbers is forbidden, the lifetime of these excitations becomes extremely long [15]. These times exceed the recombination times of a photoexcited hole by approximately 10^7 times (in a standard 2D ES, they are about 100 ps). Because of such long lifetimes, it is possible to produce the high densities of nonequilibrium spin-cyclotron excitons of $\sim 10^{10}$ cm^{-2} with the help of comparatively low-power continuous photoexcitation. [4]

Spin-cyclotron excitons are purely electron excitations, but they can be called composite bosons because they have the integer spin ($S = 1$) and follow in fact the Bose statistics: a macroscopically large number of excitons can be found in one quantum state. In a collective of spin-cyclotron excitons, the formation of nonequilibrium boson condensates, which were formally studied already in [33], could be expected. However, it is known that thermal fluctuations in two-dimensional (and one-dimensional) spatially infinite systems destroy the long-range order at any arbitrarily low but finite temperature [34, 35]. For this reason, a Bose condensate in such systems can exist only at $T = 0$, which is of no more than theoretical interest.

Nevertheless, thermal fluctuations in the 2D case do not destroy completely the long-range order. Spatial electron–electron correlations are preserved, although they decrease with distance not exponentially, as in a gas phase, but according to a power law. This proves to be sufficient for a transition to a new phase which can exhibit superfluidity at a finite temperature. The superfluidity effect in 2D systems without Bose condensate formation was predicted by Berezinskii [36, 37] and, independently, later by Kosterlitz and Thouless [38] (the Berezinskii–Kosterlitz–Thouless (BKT) transition). According to the theory, the transition to the superfluid state in this case is caused by the formation of topological defects: vortex–antivortex pairs. By now, the BKT transition has been observed in many quasi-two-dimensional systems: liquid helium films [39, 40], Josephson-contact arrays [41], cooled atomic gases [42, 43], and a gas of interacting exciton polaritons [44]. A high-density ensemble of spin-cyclotron excitons in a quantum Hall insulator ($\nu = 2$) at temperatures below 1 K may be another example of a dense Bose system in a degenerate two-dimensional Fermi gas demonstrating collective Bose properties along with electron–electron bilayers [45].

Note that the search for Bose–Einstein condensates is one of the central focuses in modern physics, first and foremost in condensed state physics. Although nontrivial phase transitions in solids that can be treated as transitions to a condensed state have been observed in many experiments, the reliably established cases of Bose–Einstein condensate formation are not numerous.

Condensate states can be divided into two fundamental groups. One of them is determined by the phase transition in the ground, thermodynamically equilibrium state, as, for example, in superfluid ^{4}He. At present, however, special interest is attracted by so-called nonstationary condensates — systems disturbed from equilibrium by an external action. Although the detailed equilibrium in such systems is not established, they can, in turn, be divided into macroscopic subsystems in which local (dynamic) 'quasi-equilibrium' appears and nonequilibrium subsystems can be in the 'quasi-equilibrium' state long enough to use the concept of temperature, while Bose–Einstein condensation could occur in the subsystem itself. Quasi-equilibrium systems include exciton-polariton condensates [46], the Bose condensate of three-dimensional magnons [47], atomic Bose condensates [48, 49], Bose condensates of 2D magnetoexcitons [33, 50], and spatially indirect dipolar excitons [51–53].

Fermion condensates, which take a special place among condensate states, can also be divided into thermodynamically equilibrium superconductors (including high-temperature superconductors), ^{3}He [54], the state with the total filling factor $\nu = 1$ in double electron layers [45], and nonequilibrium systems such as a condensate of cooled ^{40}K atoms initially following the Fermi statistics [55].

In this review, we discuss a condensate in a system of 2D fermions (2D electrons in the conduction band) disturbed from equilibrium due to the formation of an ensemble of long-lived spin-cyclotron excitons — composite excitations with the Bose statistics.

Note that purely electron magnetoexcitons of all types considered here also possess electron-hole symmetry: the mass and charge of the excited electron are equal to the mass and charge (with the opposite sign) of the effective Fermi hole. Thus, the spatial transfer of magnetoexcitons involves neither the charge transfer nor the mass transfer (the local electron density does not change during the transfer process) but is related only to the magnetoexciton excitation energy and spin transfer. Upon condensation of such excitations into a coherent collective state, a nondissipative propagation of the spin over macroscopic distances can be expected. The experimental study of the nondiffusion spreading of a magnetoexciton condensate is discussed in Section 8.

In this review, we discuss optical methods that we developed to form dense ensembles of spin excitations and to measure their relaxation times in a quantum Hall ferromagnetic ($\nu = 1$) and a quantum Hall insulator ($\nu = 2$). The formation of dense boson subsystems of spin excitations in a strongly correlated 2D ES is considered. The main research methods are resonance Rayleigh scattering, photo-induced resonance reflection, and photoluminescence. Because neither of these methods can be applied for studying the relaxation of Goldstone excitons in a quantum Hall ferromagnet ($\nu = 1$), their relaxation times were measured by the method of time-resolved Kerr rotation [56].

[4] The power is low compared to that required for heating a 2D ES to a temperature exceeding the GaAs lattice temperature.

2. Rayleigh scattering of light by two-dimensional electrons in a strong magnetic field

Since its very discovery, Rayleigh scattering [57] has been one of the most powerful spectroscopic methods for studying the local properties of inhomogeneous media [58], in particular, for determining the critical fluctuations of the order parameter during phase transitions in liquids and solids [59]. In resonance Rayleigh scattering (RRS), when the scattered light energy coincides with the energy of the allowed optical transition, the scattering cross section drastically increases. Resonance Rayleigh scattering at magnetoexciton transitions is successfully used to study inhomogeneously broadened optical transitions in quantum wells (QWs) [60–62]. The RRS method was recently applied for observations of new correlated phases in the ground state of 2D ESs [63–65].

Resonance Rayleigh scattering was used for the first time in [66] to measure the spin polarization of electrons in 2D ESs. The RRS and photoluminescence (PL) spectra were obtained using the two-beam method (see the inset in Fig. 1a). The radiation from a Ti-sapphire laser was delivered through a fiber onto a sample placed in a helium cryostat. The second fiber collected Rayleigh scattering and PL signals and delivered them to a spectrometer. Measurements were performed at temperatures from 0.4 to 4.2 K in magnetic fields from 0 to 14 T. A set of samples with high quality doped single $GaAs/Al_xGa_{1-x}As$ QWs with the same width of 19 nm was studied. The electron concentration n_e in the QWs was varied in the range of $(0.5-2.4)\times 10^{11}$ cm^{-2} with the mobility $\mu_e = 5\times 10^6$ cm^2 V^{-1} s^{-1}. The electron density was measured by the PL signal from the 2D ES.

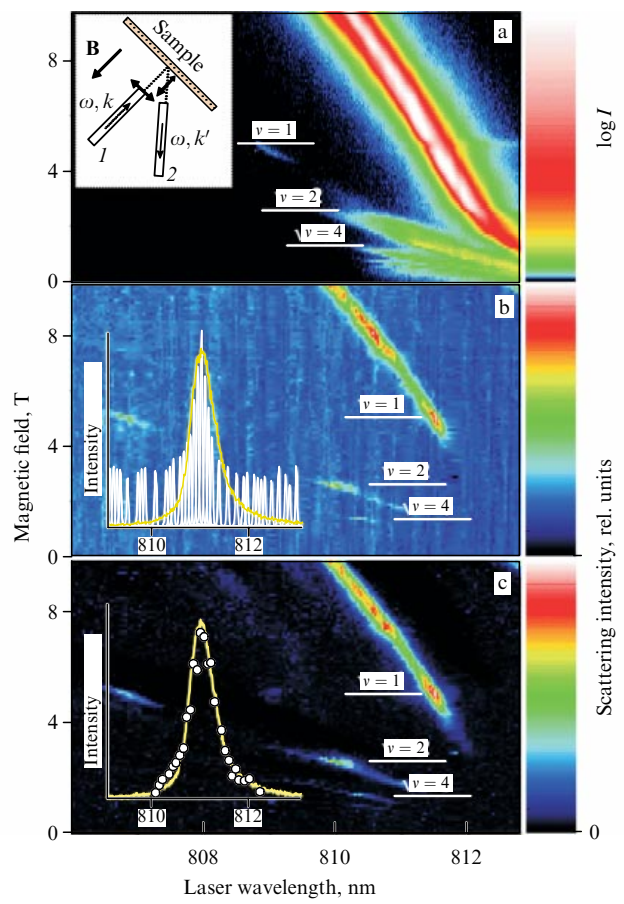

Figure 1. (Color online.) (a) Logarithm of the PL intensity for a 2D ES in a magnetic field. Magnetic fields determined from PL spectra corresponding to integer filling factors are indicated. The inset shows the geometry of experiments. (b) The RRS amplitude measured in the same spectral and magnetic field ranges as PL in Fig. 1a. The Ti:sapphire laser power density is 10 mW cm^{-2}; the RRS spectra were recorded with an accumulation time of 0.1 s. The inset shows an RRS spectrum for $\nu = 1$ with the corresponding PL line. (c) The differential RRS signal amplitude. The inset shows a differential RRS spectrum for $\nu = 1$ with the corresponding PL line.

In the measurement of RRS, the contribution of scattering from the sample surface was suppressed with the help of a pair of crossed linear polarizers placed between the ends of the fibers and the sample. Because the polarization of photons scattered by the surface is the same as for exciting photons, while a 2D ES in a magnetic field absorbs (emits) circularly polarized light due to the breakdown of time reversal symmetry, the signal of linearly polarized nonresonance Rayleigh scattering from the sample surface decreased by almost two orders of magnitude. To remove the remnants of Rayleigh scattering from the sample surface, thereby additionally suppressing the background signal of nonresonance Rayleigh scattering, a differential method was used. A sample under study was irradiated by an He-Ne laser, reducing the electron density [62]. The He-Ne laser radiation was tuned so that RRS lines for the photodepleted and nondepleted states do not overlap. By subtracting one signal from another, it was possible to increase the signal-to-noise ratio by a further order of magnitude (Fig. 1c).

Photoluminescence and RRS spectra have much in common. However, a significant difference is that intermediate states are real for PL and virtual for RRS. In the lowest-order perturbation theory, RRS corresponds to the absorption of a photon and the creation of a virtual electron-hole (e–h) pair. Then, the e–h pair is annihilated, emitting a scattered photon [67, 68]. Scattering of this type is possible only for localized e–h pairs with the localization length Λ much smaller than the wavelength λ of scattered light, i.e., $k_{\parallel}\Lambda \ll 1$ (where $k_{\parallel}$ is the projection of the photon wave vector on the 2D ES plane). This condition is fulfilled for the localized states of a 2D ES in a magnetic field [69]. In addition, the condition $l_B \ll \Lambda$ is fulfilled in a strong magnetic field B. The value of Λ for most of the states at the Landau level is in no way related to a magnetic field, being determined by the correlation length of spatial fluctuations of a random smooth potential inevitably present in the 2D channel of a real semiconductor heterostructure. For this reason, the matrix element of the radiative (dipole) transition to a virtual state determined by the scale Λ is independent of the magnetic field. If localized states are distributed randomly, the RRS cross section is proportional to the number of scattering states and the probability of an individual process [67, 68].

Apart from the obvious light scattering process involving localized electron states, Rayleigh scattering involving delocalized states is not forbidden either. The law of conservation of momentum is fulfilled for the system, consisting of the incident photon, the scattered photon, and 2D electrons, due to Coulomb interaction of the electron of a virtual electron-hole pair and electrons of the 2D gas. Therefore, Rayleigh scattering involving delocalized states can be active only for partially-filled electronic levels.

Experimental data [66] unambiguously indicate the RRS mechanism in 2D ESs in quantizing magnetic fields. Resonance Rayleigh scattering was studied in a 2D ES with one partially filled spin sublevel of the zero Landau level at

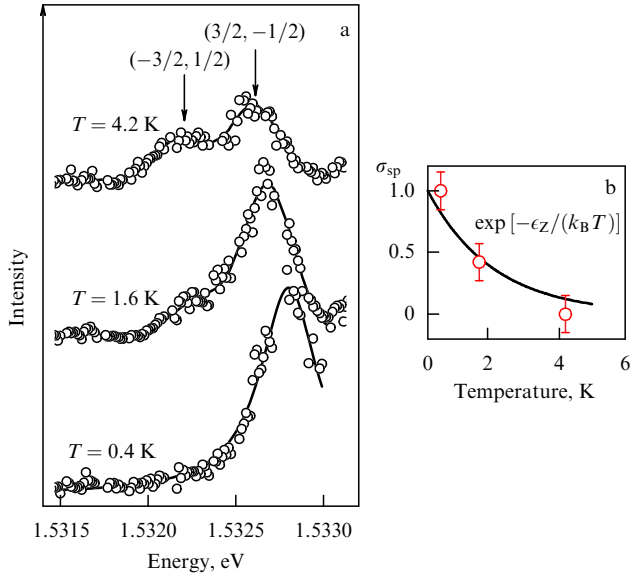

Figure 2. (a) RRS spectra at three temperatures for $\nu = 0.36$. (b) Spin polarization of delocalized 2D electrons as a function of temperature: experiment (circles) and an analytic curve for the thermodynamic electron distribution among spin sublevels $\sim \exp[-\epsilon_Z/(k_B T)]$ (solid curve).

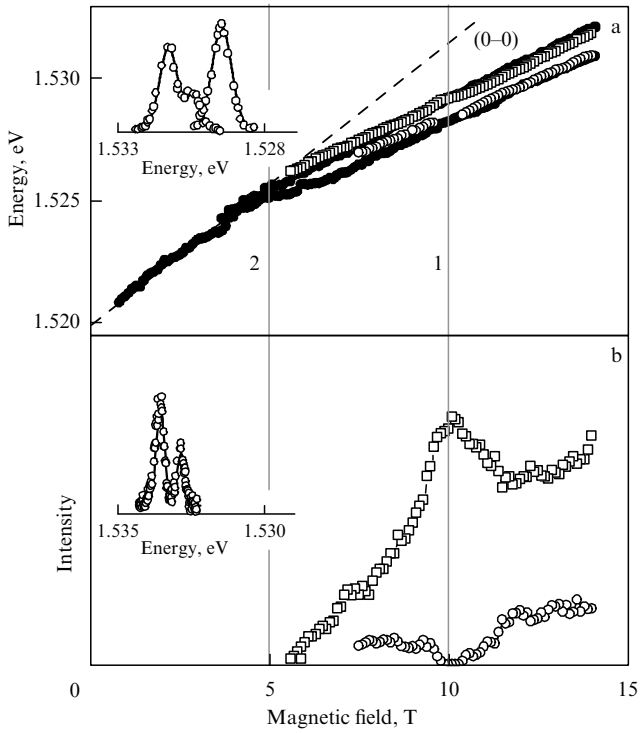

Figure 3. (a) PL (filled circles) and RRS (empty circles) line energies for a sample with the electron concentration $n_e = 2.4 \times 10^{11}$ cm^{-2}. The dashed line shows the energy of 0–0 electron-hole transitions for electron and hole masses of $0.067m_e$ and $0.2m_e$, respectively. The electron filling factors are shown by vertical lines. The inset shows RRS spectra measured in magnetic fields of 10 T ($\nu = 1$) and 13 T ($\nu \approx 0.83$) (circles) and their Gaussian approximations (solid curves). (b) Magnetic field dependences of the integrated RRS signal intensities for optical transitions involving electronic states with different spins: states from the lower (circles) and upper (squares) spin sublevels of the zero Landau level. The inset presents the RRS spectrum of a sample with an undoped QW in the field 13 T (circles) and its Gaussian approximation (curve). The ratio of areas under the RRS lines gives $f_\uparrow/f_\downarrow$.

temperatures considerably lower than single-particle Zeeman splitting ϵ_Z. The presence of the only intense Rayleigh line with the participation of electronic states at the empty upper spin Landau sublevel and the absence of scattering with the participation of states at the partially filled lowest spin Landau sublevel suggests that scattering occurs on localized electrons. The decrease in the contribution to the RRS intensity caused by the states at the upper spin Landau sublevel with increasing temperature (Fig. 2a) is explained by the partial filling of localized states at the upper Landau level, while the appearance of scattering caused by the states at the lower spin Landau sublevel is related to the partial depletion of localized states at the lower Landau level.

From relative integral intensities of two RRS lines from two different spin states at the zero Landau level (Fig. 3) it is possible to determine the spin polarization of electrons $\sigma_{sp} = (\nu_\uparrow - \nu_\downarrow)/\nu$ in the ultraquantum limit $\nu \leqslant 2$ [66] (here, $\nu_{\uparrow/\downarrow}$ are filling factors for up/down spins at the zero Landau level; $\nu = \nu_\uparrow + \nu_\downarrow$). Indeed, since the integrated intensities (areas under RRS lines) are proportional to the number of vacancies at spin sublevels of the zero Landau level, $I_\uparrow = Cf_\uparrow(1 - \nu_\uparrow)$ and $I_\downarrow = Cf_\downarrow(1 - \nu_\downarrow)$ ($f_\uparrow$ and $f_\downarrow$ are scattering cross sections for corresponding transitions, which are assumed to be constant because the RRS lines are narrow), we find

$$\sigma_{sp} = \frac{2 - \nu}{\nu} \, \frac{I_\downarrow f_\uparrow - I_\uparrow f_\downarrow}{I_\downarrow f_\uparrow + I_\uparrow f_\downarrow} \, .$$

Resonance Rayleigh scattering cross sections were obtained directly in RRS experiments for a similar sample without electrons in the conduction band of a QW (see the inset in Fig. 3b), so that, to determine σ_{sp}, it is sufficient to know only the ratio of $f_\uparrow$ and $f_\downarrow$. In the magnetic field range from 8 to 14 T, this ratio changes linearly from 2.2 to 1.8. The spin polarization σ_{sp} can be obtained from the known ratio $f_\uparrow/f_\downarrow$ (Fig. 4).

Thus, RRS can be used as a noninvasive optical method for probing the spin polarization of 2D ESs [70]. This is very important because, for measuring the absorption or transmission of a 2D ES, a sample with a high-quality epitaxial heterostructure grown on a single-crystal substrate should be greatly modified [71, 72].

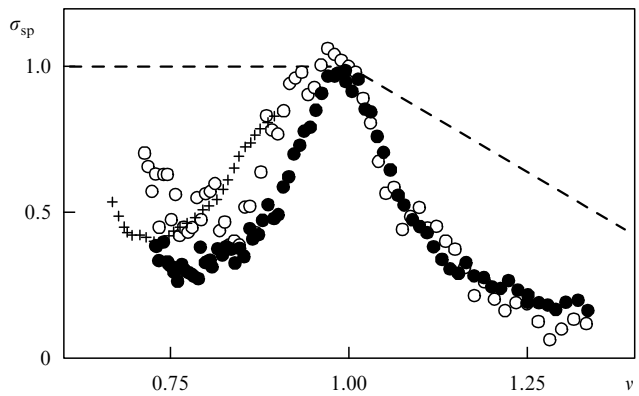

Figure 4. Spin polarization of a 2D ES (S_z) calculated using experimental data presented in Fig. 3 (empty circles). For comparison, the values of S_z from [71, 72] are presented (filled circles and crosses, respectively). The dashed line shows the degree of spin polarization of the 2D ES for noninteracting electrons.

At present, high-quality transmission spectra are obtained either by etching a hole in a substrate to remove parasitic bulk scattering [71, 73] or by growing a Bragg mirror separating the 2D ES from the substrate [72, 74].

Among noninvasive optical methods for measuring the spin polarization, we mention elegant experimental methods using the recombination of free electrons with localized acceptors [75] and magnetoexciton dichroism measurements [72]. However, these methods have a number of significant limitations complicating the interpretation of experimental data. An argument in favor of RRS is that the spin polarization is measured without any preliminary processing of samples, and experimental results are consistent with other known data on 2D ES polarization in the ultraquantum limit. In addition, as shown in Section 3, the RRS method for measuring the spin polarization can be readily used for time-resolved measurements to control the evolution of the spin polarization of 2D ESs after pulsed excitation in the real-time regime.

3. Spin relaxation in a quantum Hall ferromagnetic state with the electron filling factor $\nu = 1$

The spin relaxation time in a spin-polarized quantum Hall ferromagnetic state was measured using an original optical method developed for creating nonequilibrium spin magnetoexcitons (see the experimental setup in Fig. 5a). A special feature of this method is the possibility of creating systems with in fact an arbitrary initial spin polarization (from 0 to 1) and observing the spin relaxation dynamics in real time. The spin state of the electron system is monitored using time-resolved RRS.

A system of nonequilibrium spins is created by 532-nm, 1-ns laser pulses producing a peak power density of $\simeq 400$ W cm^{-2} on a sample. Photoexcited high-energy electrons relaxing to the ground state heat the 2D ES. Therefore, the experiment itself is meaningful when the characteristic time required for cooling the 2D ES to the ambient temperature is considerably shorter than the spin relaxation time τ (otherwise, the relaxation time cannot be measured accurately). It was found that this condition can be satisfied in magnetic fields $B > 8$ T. The optically heated 2D ES cools down and relaxes during cooling to a partially polarized quasi-equilibrium state, which then relaxes to the ground spin-polarized state. Aside from pulsed excitation, the 2D ES is excited by cw resonant laser radiation (see Fig. 5).

As mentioned in Section 2, the intensity ratio of the RRS lines from electronic states with different spins allows one to control in real time the spin relaxation dynamics by varying the time delay of RRS recording with respect to the 532-nm exciting laser pulse. The spin relaxation time measured in this way (Fig. 6) proved to be at least an order of magnitude longer than relaxation times obtained by alternative experimental methods [7–10]. The method presented here measures directly the energy relaxation of the spin from the upper spin sublevel to lower spin sublevels, whereas other experimental methods measure the dephasing (stochastization) of the spin of one or several noninteracting spin magnetoexcitons.

It is important that the experimental method described here does not cause any rotation of the spin of the whole system, i.e., the initial spin deviation from the ground spin-polarized state is related only to the change in the total spin,

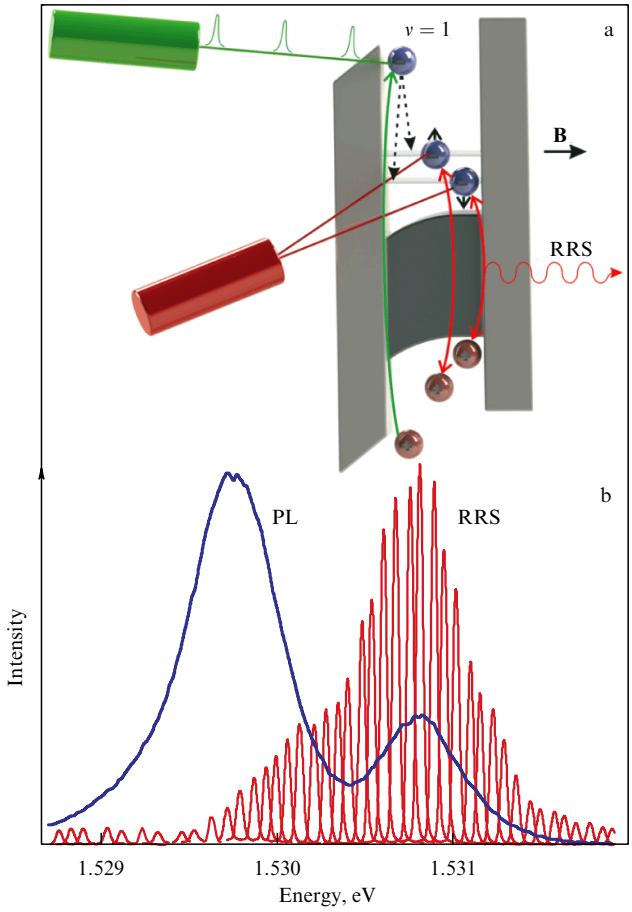

Figure 5. (a) Diagram illustrating the experimental setup. (b) PL and RRS spectra recorded 5 ms after a laser pulse after the end of all relaxation processes. $B = 11$ T; reservoir temperature is $T = 1.6$ K.

which nevertheless always remains directed along the magnetic field. As pointed out earlier, such a deviation corresponds to excitation of only spin-wave excitons $X_{\mathbf{q}}$ in the system, but not Goldstone excitons (X_G).

Theoretical studies of the spin relaxation in quantum Hall systems [11–15, 76–81] have shown that this process involves a variety of different relaxation mechanisms, which greatly complicates the determination of the dominating relaxation channel. Moreover, the relaxation picture can substantially change depending on the magnetic field strength, temperature, and filling factor. At the same time, it is clear that the relaxation/annihilation of spin magnetoexcitons requires the presence of interactions of two types: (1) interactions not preserving the system spin and (2) interactions providing the irreversibility of the relaxation process.

Analysis shows that the interaction of the first type can be the spin-orbit interaction in the 2D channel [12–15, 76–79, 81] and/or the hyperfine interaction with lattice nuclei [14, 80].

The dissipative mechanism can be realized: (1) in the efficient Coulomb (in fact, electric dipole-dipole) interaction of magnetoexcitons resulting, e.g., in the coalescence of spin-wave excitons (when two excitons transform into one with addition of their energy and momentum (see [77, 79])); (2) in the interaction of electrons with an external smooth potential also leading to coalescence, but with the increased phase volume involved in the relaxation of magnetoexcitons due to

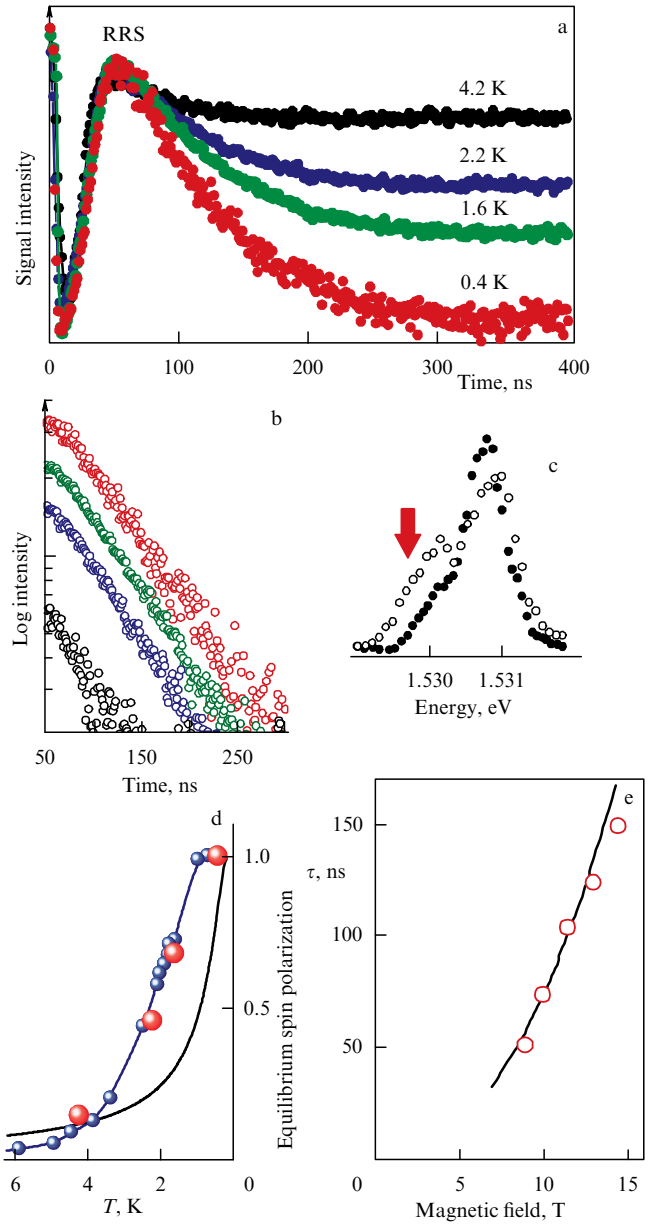

Figure 6. (Color online.) (a) RRS dynamics at temperatures of 0.4, 1.6, 2.2, and 4.2 K. The RRS signals at different T are normalized to obtain equal intensities 50 ns after the heating laser pulse. (b) RRS kinetics after the subtraction of the saturation signal on a logarithmic scale at different T (colors of symbols are the same as in Fig. 6a). (c) Nonequilibrium (empty circles) and equilibrium (filled circles) RRS spectra measured 50 ns and 5 ms after the heating laser pulse, respectively. The arrow shows the position of the maximum of PL line for the e–h transition related to the lowest Landau electron spin sublevel where the RRS signal dynamics is measured. $B = 11$ T, $T = 1.6$ K. (d) Equilibrium spin polarization (large circles) obtained using the RRS saturation amplitude at different T (the equilibrium polarization at 0.4 K is assumed equal to unity). For comparison, we present the equilibrium spin polarization measured by the nuclear spin resonance (NSR) method in [82] for the same Zeeman splitting of spin sublevels (small circles connected by a thin line). The thick line is the equilibrium one-particle spin polarization disregarding the Coulomb interaction. (e) Magnetic-field dependence of the relaxation time $\tau(B)$: experiment (circles) and calculation (curve).

nonconservation of momentum in this process [13, 78, 79]; and (3) in the electron-phonon interaction leading to energy dissipation due to emission/absorption of phonons [12, 14, 15, 76, 79, 80].

A comparative analysis of various temperature-independent channels of spin-wave exciton relaxation in a quantum Hall ferromagnet (i.e., corresponding to the longitudinal spin relaxation of the electron system) was performed in [14]. The estimate showed that, for the filling factor $\nu = 1$ in sufficiently large magnetic fields up to $B = 15$ T, the relaxation channel should be determined by the spin-orbit interaction providing the spin change and by interaction with a smooth random potential breaking the conservation of momentum. At the same time, it was assumed that the random potential is fairly weak and does not affect the energy spectrum of spin-wave excitons or their energy distribution. In this case, the two-exciton mechanism of scattering dominates, which leads to the nonexponential relaxation law $\sim 1/(1 + t/\tau)$ [13, 14].

Later experiments performed using the above method [83] showed that the observed relaxation nevertheless has an exponential time dependence. This required additional theoretical study taking into account more realistic conditions, in particular, obviously a greater role of spatial fluctuations of the external potential present in the 2D channel. (A considerable role of 'disorder' is also indirectly demonstrated by a comparatively low dark mobility of $(1-3) \times 10^6$ cm^2 V^{-1} s^{-1} in samples with wide QWs studied in these experiments.)

The theoretical method, as in Refs [12–15, 76–80], is based on the use of the 'exciton representation' basis playing the role of the 'correct zero-approximation basis' and simplifying the perturbative approach in calculations of spectra and relaxation processes in integer quantum Hall systems.

Note that the mechanism considered here and in [83] is temperature-independent, i.e., it dominates at quite low temperatures (an estimate will be presented below). Experiments also showed that the relaxation rate was independent of temperature (Fig. 6b).

In our opinion, the most efficient mechanism under experimental conditions [83] is based on the elementary process corresponding to a transition in the continuous spectrum of a quantum-mechanical system, namely, to the two-exciton scattering $X_{\mathbf{q}_1} + X_{\mathbf{q}_2} \to X_{\mathbf{q}'}$ at which, instead of two spin-wave excitons $X_{\mathbf{q}_1}$ and $X_{\mathbf{q}_2}$, a third one appears with the total energy $E_{\mathbf{q}'} = E_{\mathbf{q}_1} + E_{\mathbf{q}_2}$. If $n_{\mathbf{q}}$ is the spatial exciton density, then for fixed $\mathbf{q}_1$ and $\mathbf{q}_2$, the probability of such an event occurring per unit time inside the domain $l \times l = A$ of the two-dimensional space is

$$w(\mathbf{q}_1, \mathbf{q}_2) = \frac{n_{\mathbf{q}_1} n_{\mathbf{q}_2} A^2}{\tau(\mathbf{q}_1, \mathbf{q}_2)} \tag{1}$$

(we ignore any correlations between excitons and the spatial inhomogeneity of the density $n_{\mathbf{q}}$ within the domain). The quantity $\tau(\ldots)$ is calculated from the known expression

$$\frac{1}{\tau(\mathbf{q}_1, \mathbf{q}_2)} = \frac{2\pi}{\hbar} \sum_{\mathbf{q}'} |\mathcal{M}(\mathbf{q}_1, \mathbf{q}_2, \mathbf{q}')|^2 \delta(E_{\mathbf{q}_1} + E_{\mathbf{q}_2} - E_{\mathbf{q}'}) \,. \tag{2}$$

The matrix element $\mathcal{M}(\ldots)$ is determined by the spin-orbit interaction in the 2D channel and the external field whose role is reduced to the nonconservation of momentum upon scattering. This matrix element was in fact already calculated in Refs [12, 76], where the nonconservation of momentum was caused by phonon emission or absorption.

In [13], an external field was represented by a smooth random potential $\varphi(\mathbf{r})$ that, generally speaking, is poorly known, except the fact that its characteristic amplitude in

modern structures is 5–12 K and the spatial fluctuation scale (correlation length) $\Lambda \simeq 30-50$ nm.

It is convenient to introduce the correlation function $K(\mathbf{r}) = \langle \varphi(\mathbf{r}+\mathbf{R})\,\varphi(\mathbf{R})\rangle_R$ (angle brackets $\langle\ldots\rangle_R$ mean averaging in the 2D space of the system under study, i.e., at scales larger than Λ; it is also assumed that the condition $\langle\varphi(\mathbf{R})\rangle_R = 0$ is fulfilled). Correspondingly, the Fourier component

$$\bar{K}(q) = \frac{1}{(2\pi)^2}\int K(\mathbf{r})\exp(-\mathrm{i}\mathbf{q}\mathbf{r})\,\mathrm{d}^2 r$$

can be introduced. Then, the square of the modulus of the matrix element of the transient process under study will have the form

$$\left|\mathcal{M}(\mathbf{q}_1,\mathbf{q}_2,\mathbf{q}')\right|^2 = 32\pi^3\bar{K}(q^*)(\alpha^2+\beta^2)\left(\frac{q^* l_B}{A\hbar\omega_c}\right)^2, \qquad (3)$$

where $\mathbf{q}^* = \mathbf{q}_1+\mathbf{q}_2-\mathbf{q}'$, ω_c is the cyclotron frequency, and α and β are the Rashba and Dresselhaus constants, respectively, determining the spin-orbit interaction for 2D electrons. This result was obtained assuming that $l \gg l_B$. Therefore, the basis states of electrons inside the domain are the usual states of a degenerate Landau level.

The scattering matrix element (3) proves to be inversely proportional to the domain area A, which follows from a simple circumstance: the smaller the region where quantum-mechanical excited states are considered (i.e., the smaller the scale at which these states are normalized), the more efficient the overlap of these states. At the same time, the substitution of (3) into (2) gives after summation over $\mathbf{q}'$ an additional factor $\propto A$, so that the total probability (1) of the annihilation of a spin-wave exciton inside a domain is, as it should be, proportional to the domain area.

If the temperature is low enough, the calculation of the total relaxation rate requires knowledge of the quasi-equilibrium distribution of 'cold' spin-wave excitons determined in the state when they are 'cooled' but not annihilated yet, because energy relaxation processes not related to the spin flip occur much faster than the spin relaxation. The problem of finding this distribution in the real space cannot be exactly solved. We will present only an estimate, based on allowing for the more substantial role of the external random potential than simply its influence on the value of the matrix element of the transition (3).

Note that in the presence of the potential $\varphi(\mathbf{r})$, the momentum of a magnetoexciton is not an exact quantum number. However, assuming that the potential is smooth and considering a domain with the characteristic size $l \ll \Lambda$ (but at the same time, $l \gg l_B$), we can use the 'gradient approximation'. This means that the field $\mathscr{E} = -\nabla\varphi$ inside the domain can be considered homogeneous. In the gradient approximation, the potential does not change the states of magnetoexcitons and conserves the quantum number $\mathbf{q}$. It is well known [23, 28, 29, 33] that any magnetoexciton has the dipole moment $\mathbf{d} = l_B^2\mathbf{q}\times\hat{\mathbf{z}}$. Therefore, the total energy of a spin-wave exciton for small momenta $ql_B \ll 1$ has the form

$$E_{\mathbf{q}} = \epsilon_Z + \frac{q^2 l_B^2}{2M_X} + l_B^2\,(\mathbf{q}\times\mathscr{E})_z\,. \qquad (4)$$

After 'cooling' (but before annihilation), this energy should be close to its minimal value. From the condition $\partial E_{\mathbf{q}}/\partial\mathbf{q} = 0$, equivalent to the zero group velocity of the spin wave, we find the 'equilibrium' exciton momentum $\mathbf{q}_m = -M_X\mathscr{E}\times\hat{\mathbf{z}}$ and the corresponding energy $\mathcal{E}_m = E_{\mathbf{q}_m} = \epsilon_Z - 1/2M_X l_B^2\mathscr{E}^2$ (here $\mathscr{E} = |\mathscr{E}|$). Thus, the energy of a spin-wave exciton 'trapped' in a smooth random potential proves to be even smaller than the Zeeman gap. Taking into account theoretical [28, 29] and experimental [84, 85] data on the exciton mass M_X, the negative correction is approximately 20–30% of the value of ϵ_Z.

Now, we estimate for the chosen domain the time $\tau(\mathbf{q}_1,\mathbf{q}_2)$ determined by expression (2). First, we set $\mathbf{q}_1 = \mathbf{q}_2 = \mathbf{q}_m(\mathbf{R})$, where the coordinate $\mathbf{R}$ gives the domain position (for example, its center position) and specifies the field strength $\mathscr{E}(\mathbf{R})$. Second, we assume that the correlator form is specified, for example, it is described by a Gaussian function: $K(R) = \Lambda^2\exp(-R^2/\Lambda^2)$. Assuming that the argument of the δ function is equal to $2\mathcal{E}_m - E_{\mathbf{q}'}$, taking into account expression (4) for energy, and passing in (2) from summation to integration , we find $1/\tau(\mathbf{q}_m,\mathbf{q}_m) \equiv \mathscr{W}(\mathbf{R})/A$, where

$$\mathscr{W}(\mathbf{R}) = \frac{4\pi(\alpha^2+\beta^2)\,M_X}{\hbar}\left(\frac{\Delta\Lambda}{\hbar\omega_c l_B}\right)^2 \times\int_{\xi_{\min}}^{\xi_{\max}}\frac{\exp\left\{-\kappa(\xi)\left[\Lambda/(2l_B)\right]^2\right\}\kappa(\xi)\,\xi\,\mathrm{d}\xi}{\sqrt{\xi_m^2\xi^2-(\xi^2/2+\xi_m^2-\epsilon_Z M_X)^2}}\,. \qquad (5)$$

Here, $\xi_m(\mathbf{R}) = M_X l_B\mathscr{E}(\mathbf{R})$, $\xi_{\min} = |\sqrt{2M_X\mathcal{E}_m}-\xi_m|$, $\xi_{\max} = \sqrt{2M_X\mathcal{E}_m}+\xi_m$, and $\kappa(\xi) = 4\epsilon_Z M_X - \xi^2$. The spin relaxation rate determined experimentally is calculated by multiplying the probability $\mathscr{W}/A$ by the probability of finding two excitons within the considered domain (1) and then by summing over all such domains, naturally turning into integration with the help of the substitution $A \to \mathrm{d}^2R$:

$$-\frac{\mathrm{d}N_X}{\mathrm{d}t} = \int n^2(\mathbf{R})\,\mathscr{W}(\mathbf{R})\,\mathrm{d}^2R\,. \qquad (6)$$

Here, $N_X(t)$ is the total number of spin-wave excitons and $n(\mathbf{R})$ is the local density equal to $n_{\mathbf{q}_m}$ $[N_X = \int n(\mathbf{R})\,\mathrm{d}^2R]$.

Thus, the spin relaxation rate depends on the spatial distribution of the random field $[\mathscr{E}(\mathbf{R})]^2 \equiv (\nabla\varphi)^2$, which should be known for calculating the probability $\mathscr{W}(\mathbf{R})$, and on the quasi-equilibrium distribution $n(\mathbf{R})$. The latter is established due to fast transient processes preceding the annihilation of spin-wave excitons, namely because of their cooling caused by electron–phonon interaction and simultaneous drift in a smooth random potential.

We will estimate integral (6) in two stages. First, we will replace $\mathscr{E}^2$ in (5) by the average $\langle\mathscr{E}^2\rangle_R = \langle(\nabla\varphi)^2\rangle_R \equiv (2\Delta/\Lambda)^2$ (this relation is valid for the Gaussian distribution of $\varphi(\mathbf{R})$). In this way, we replace $\mathscr{W}$ in integral (6) with the quantity $\overline{\mathscr{W}}$ independent of $\mathbf{R}$: $-\mathrm{d}N_X/\mathrm{d}t \sim \overline{\mathscr{W}}\int n^2(\mathbf{R})\,\mathrm{d}^2R$. Second, for a spatially fluctuating density $n(\mathbf{R}) \equiv \langle n\rangle_R + \delta n(\mathbf{R})$, we evaluate the integral $\int n^2(\mathbf{R})\,\mathrm{d}^2R \equiv N_X\bar{n} + \int[\delta n(\mathbf{R})]^2\,\mathrm{d}^2R$ (here $\bar{n} \equiv \langle n\rangle_R$ is the average density of spin-wave excitons, $\langle\delta n\rangle_R = 0$). The term $\int(\delta n)^2\,\mathrm{d}^2R$ is proportional to the spatial correlator $\langle\delta n(\mathbf{r}+\mathbf{R})\,\delta n(\mathbf{R})\rangle_R$ for $r = 0$. For ideal exciton gas in homogeneous space, this correlator would correspond to so-called white noise and would be equal to $\delta(\mathbf{r})\,\bar{n}$ [86]. In our case, correlations are mainly determined by spatial fluctuations of the field $\mathscr{E}^2$ (we ignore the interaction between excitons); namely, if it is energetically advantageous to find a spin-wave exciton at the point $\mathbf{R}_0$, the density should be higher than the average value, $\delta n(\mathbf{R}_0) > 0$, in the vicinity

$|\mathbf{R}-\mathbf{R}_0| \lesssim \Lambda'$. To estimate $\delta(\mathbf{r})$, we replace it by a 'cap', $\exp(-r^2/\Lambda'^2)/(\pi\Lambda'^2)$. We assume that the correlation length of the spatial distribution $(\nabla\varphi)^2$ is approximately half of that of the potential $\varphi : \Lambda' \simeq \Lambda/2$. As a result, we obtain the estimate $\int[\delta n(\mathbf{r})]^2\,\mathrm{d}\mathbf{r} \sim 4N_{\mathrm{X}}/(\pi\Lambda^2)$.

Thus, the relaxation rate $-\mathrm{d}N_{\mathrm{X}}/\mathrm{d}t$ has two components: quadratic and linear in $\overline{n}$. For the unit area, we obtain the rate of annihilating spin-wave excitons

$$-\frac{\mathrm{d}\overline{n}}{\mathrm{d}t} \sim \overline{\mathscr{W}}\left(\overline{n}^2 + \frac{4\overline{n}}{\pi\Lambda^2}\right). \tag{7}$$

As mentioned above, the theoretical approach used here ignores correlations between excitons. We assume that $\overline{n}$ is small, and therefore the second term in (7) dominates. The experimentally observed relaxation is exponential in time even if the initial value $\overline{n}(0) \simeq 0.5/(2\pi l_B^2)$ is used ($1/(2\pi l_B^2)$ is the density of spin-polarized electrons in a quantum Hall ferromagnet).

Thus, we conclude semiempirically that the characteristic relaxation time is determined by the expression $\mathcal{T} = \pi\Lambda^2/(4\overline{\mathscr{W}})$. As for the parameters of the material, we can estimate them using data for similar QWs [87] and varying poorly known quantities Δ and Λ in the vicinity of their experimentally estimates values. The amplitude Δ is borrowed from experiments [88, 89].

To compare theoretical results with experimental data, we can choose the following material parameters, which are quite realistic under our experimental conditions: $\alpha = 0.25$ nm meV, $\beta = 0.12$ nm meV, $\epsilon_{\mathrm{Z}} = 0.02B$ meV, $1/M_{\mathrm{X}} = 0.87B^{1/2}$ meV (where B is measured in tesla), $\Delta = 1.05$ meV, and $\Lambda = 38$ nm. As a result, the dependence $\mathcal{T}(B)$ is obtained, which well describes the experimental data (Fig. 6e). Finally, note that the real temperature at which the temperature-independent relaxation channel operates should be of the order of or lower than the 'localization energy' of a spin-wave exciton in a smooth random potential: $T \lesssim M_{\mathrm{X}} l_B^2 \mathscr{E}^2 \sim 4M_{\mathrm{X}}(l_B\Delta/\Lambda)^2 \simeq 0.8-1.3$ K.

Thus, we have shown for the first time that the relaxation times of spin magentoexcitons in a quantum Hall ferromagnet ($\nu = 1$) are consistent with their theoretical values (Fig. 6e) and exceed experimental relaxation times measured earlier by more than an order of magnitude. However, these results do not give to date a complete picture of the spin relaxation, because the excited states of a quantum Hall ferromagnet are not only the spin-wave excitons considered above but also Goldstone spin excitons changing the spin quantum numbers of the electronic system by $\delta S = 0$ and $\delta S_z = -1$, which corresponds to the deviation of the total spin by some angle from the magnetic field direction.

4. Relaxation of the transverse spin component in a quantum Hall ferromagnet. The stochastization of a Goldstone mode

The deviation of the total spin of an electron system by some angle $0 < \theta < \pi$ from its direction in the equilibrium state, close to the ground state, is a macroscopic Goldstone mode. In this case, the rotational symmetry of the spin system changes spontaneously from the continuous $\mathrm{C}_{\infty\mathrm{v}}$ group (with respect to rotations around the $\hat{z} \parallel \mathbf{B}$ axis) to the trivial cyclic $\mathrm{C}_{1\mathrm{v}}$ group. It is important that such a purely spin deviation does not change the orbital state of the 2D ES. The excited mode energy is $\epsilon_{\mathrm{Z}}(1-\cos\theta)\,S(0)$ (where $S(0)$ is the total spin at the initial moment of time), i.e., it macroscopically becomes gapless in terms of the parameter θ. This state is nonstationary even in the absence of any dissipative processes: the spin evolution in the principal approximation represents precession described by the equation $\partial\mathbf{S}/\partial t = -g\mu_{\mathrm{B}}\mathbf{S}\times\mathbf{B}$, which is reduced to $\partial S_z/\partial t = 0$ and $\partial\mathbf{S}_\perp/\partial t = -g\mu_{\mathrm{B}}\mathbf{S}_\perp\times\mathbf{B}$. Historically, like the relaxation of spin waves, the transverse spin relaxation in a quantum Hall ferromagnet was studied only theoretically in the absence of any real experimental data. Here, we also first consider some main theoretical concepts required for a microscopic description and study of the further evolution of the Goldstone mode.

The transverse component $\mathbf{S}_\perp = (S_x, S_y)$ appears when microscopic excitations correspond to changes in the spin quantum numbers at which $|\delta S| < |\delta S_z|$. Obviously, these are not spin-wave excitons but states generated by the action of the operator $\hat{S}_- = \hat{S}_x - \mathrm{i}\hat{S}_y$ on the ground state of a quantum Hall ferromagnet,

$$|0\rangle = |\overbrace{\uparrow\uparrow\uparrow\ldots\uparrow}^{\mathcal{N}_\phi}\rangle\,,$$

where $\mathcal{N}_\phi$ is the number of states at the Landau level with the same spin. The n-fold action of this operator creates the stationary eigenstate $|n\rangle = (\hat{S}_-)^n|0\rangle$ with the same orbital wave function and the same total spin $S = \mathcal{N}_\phi/2$ as for $|0\rangle$, but $S_z = \mathcal{N}_\phi/2 - n$, and the energy is $E_0 + \epsilon_{\mathrm{Z}}n$, where E_0 is the ground state energy. (This statement is valid, of course, if any perturbations not conserving spin numbers S and S_z are disregarded.)

Moreover, any combination of such states $\sum_n C_n|n\rangle$ specified by a set of coefficients $\{C_n\}$ is also a state with the orbital wave function and the total spin S equal to that in the ground state. At the same time, if the number of terms in this sum is greater than one, it no longer corresponds to any eigenstate of the Hamiltonian even if the interaction in it not conserving spin is disregarded. Generally speaking, for this superposition of different eigenstates, even no direction $\hat{z}'$ in the spin space exists for which the spin projection $S_{z'}$ on it would be the eigenstate quantum number (i.e., the spin would have a certain value in this direction [5]).

Nevertheless, such a combination can be used as the initial condition for solving the nonstationary Schrödinger equation $\mathrm{i}\partial|N,t\rangle/\partial t = \hat{H}|N,t\rangle$ (hereafter, we assume that $\hbar = 1$). As a result, by ignoring all the Hamiltonian terms not commuting with operators $\hat{S}_z$ and $\hat{\mathbf{S}}^2$, we obtain a solution in the form

$$|N,t\rangle = \exp(-\mathrm{i}E_0 t)\sum_{n=0}^{N} C_n \exp(-\mathrm{i}n\epsilon_{\mathrm{Z}}t)\,|n\rangle\,. \tag{8}$$

($|0,0\rangle \equiv |0\rangle$). This expression gives the most general microscopic description of the Goldstone mode in the absence of decay. The number $N \leqslant \mathcal{N}_\phi$ is the number of the 'leader' of the basis states $|n\rangle$ used. By calculating the quantum-mechanical average of the operator $\hat{S}_+ = \hat{S}_x + \mathrm{i}\hat{S}_y$ in state (8) (which we assume to be normalized, $\langle t,N|N,t\rangle = 1$, due to the proper choice of coefficients C_nn), we find the transverse spin at the moment t:

$$\begin{aligned} S_\perp(t) &= \langle t,N|\hat{S}_+|N,t\rangle \\ &= \exp(-\mathrm{i}\epsilon_{\mathrm{Z}}t)\sum_{n=0}^{N-1} C_n^* C_{n+1}\langle n+1|n+1\rangle\,, \end{aligned} \tag{9}$$

[5] Such states in quantum mechanics are called partially spin-polarized states [90].

which corresponds to precession with the frequency $\epsilon_Z/\hbar$. The tilt angle with respect to the $\hat{z}$-axis is defined as $\theta = \arcsin(|S_\perp|/S) \equiv \arcsin(2|S_\perp|/\mathcal{N}_\phi)$. Various microscopic states (8) can macroscopically formally correspond to the same Goldstone mode. Indeed, the same value of θ can be obtained for completely different sets $\{C_n\}$, because, for the specified value of the angle for a macroscopically large number of coefficients C_n, only two conditions exist: (1) the condition $\sum_n C_n^* C_{n+1} \langle n+1|n+1\rangle = (\mathcal{N}_\phi/2)\sin\theta$ and (2) the normalization condition $\sum_n |C_n|^2 \langle n|n\rangle = 1$.

Particular cases of the state (8) were theoretically considered, of course, earlier as well. In [12, 76] and later in [13], the relaxation of an arbitrary basis state was studied (the case $C_n = \delta_{n,n_0}$). Formally, there is no any precession dynamics for such a state, because it is stationary ($S_\perp = \langle n|S_+|n\rangle \equiv 0$). At the same time, the relaxation problem in such a formulation makes sense. It is clear intuitively that for the macroscopic Goldstone mode corresponding to deviation by the angle θ, the main contribution to superposition (8) is made only by a small vicinity of quantum states near some value $n_0 = |\delta S_z| = \mathcal{N}_\phi(1-\cos\theta)/2$, i.e., the norm $|C_n|^2\langle n|n\rangle$ should have a sharp maximum at $n \approx n_0$. Therefore, it is sufficient to solve a kinetic problem of annihilation of Goldstone excitons X_G in a condensate, which is described quantum-mechanically by some state $|n\rangle$ with the number n close to the maximum. In [13, 76], the transformation of two Goldstone excitons of a condensate into one spin-wave exciton was considered:

$$n\mathrm{X_G} \to (n-2)\,\mathrm{X_G} + \mathrm{X_{\mathbf{q}}}\,. \tag{10}$$

Spin states were not conserved because of spin-orbit interactions, and process irreversibility was provided by accounting for phonon emission/absorption [12, 76] or by translation invariance breakdown due to the presence of a smooth random potential [13]. The nonexponential relaxation law was predicted. The calculated characteristic time in the first case was 1–10 μs, and in the second case 100 ns. Indirect data and subsequent direct experiments [8, 9, 56] have shown that this time is much shorter ($\lesssim 10$ ns).

Another particular case is considered in paper [91], where the relaxation of mode (8) was studied under the condition that it corresponds to the complete polarization of all spins along some $\hat{z}'$-axis tilted with respect to the $\hat{z}$-axis by a certain angle β. Then, the spin state of each polarized electron (see [90]) is

$$|\nearrow\rangle = \begin{pmatrix} \cos\dfrac{\beta}{2} \\ -\sin\dfrac{\beta}{2} \end{pmatrix}, \text{ rather than } |\uparrow\rangle = \begin{pmatrix} 1 \\ 0 \end{pmatrix}$$

and as the initial state, which is completely 'obliquely' polarized, the state

$$|\overbrace{\nearrow\nearrow\nearrow\ldots\nearrow}^{\mathcal{N}_\phi}\rangle$$

was considered. We can show that in terms of our $|n\rangle$ vector basis this state is equivalent to $|\mathcal{N}_\phi, 0\rangle = \sum_{n=0}^{\mathcal{N}_\phi} C_n|n\rangle$, where coefficients $C_n = [\cos(\beta/2)]^{\mathcal{N}_\phi - n}[-\sin(\beta/2)]^n/n!$. (By calculating $S_\perp$ from expression (9), we see that in this case the tilt angle θ is exactly equal to β.) In this purely theoretical paper, the possibility of creating such a completely 'obliquely' polarized state in a quantum Hall ferromagnet was not discussed, and only the relaxation problem was considered. It seems unlikely that the mechanism involving the direct actions of phonons on the spin chosen by the authors can be efficient in real 2D ESs. For correct numerical estimates, this channel gives even longer relaxation times than those predicted by mechanisms considered in papers [12, 13, 76] (see the discussion in [92, 93]).

The main experimental difficulty is the creation itself of such a 'spin-rotated' Goldstone mode in which the transverse component $S_\perp$ would be sufficiently noticeable. The excitation time of such a macroscopic but nonequilibrium state should be at least much shorter than the spin-precession relaxation time in 2D ES and be comparable with the precession period h/ϵ_Z or even shorter. Therefore, the use of optical excitation in experiments [8, 9, 56] is natural. The initial state is produced by a short laser pulse directed at an angle β with respect to $\mathbf{B} \parallel \hat{z}$. All photons in this pulse are circularly polarized and coherent (Fig. 7c). The 2D ES state with the zero momentum ($q = 0$) (i.e., orbitally the same as

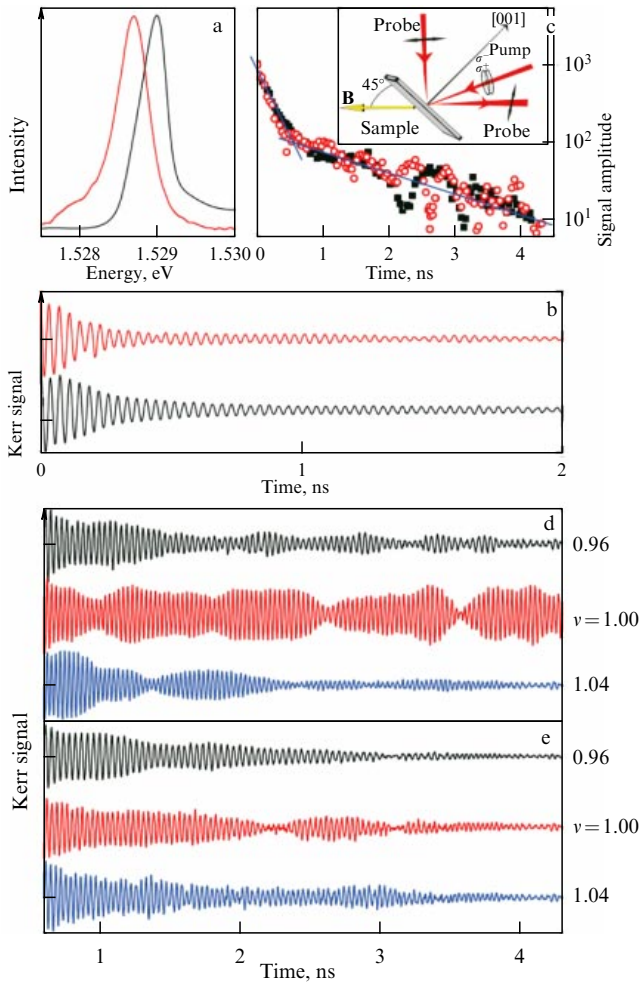

Figure 7. (Color online.) (a) PL spectrum corresponding to the optical transitions $(1/2; -3/2)$ (red curve) and $(-1/2; 3/2)$ (black curve) from the zero Landau level of the conduction band of the 2D ES to the zero Landau level of heavy holes in the valence band in a magnetic field of 4.3-T ($\nu = 0.96$). (b) Time-resolved Kerr rotation signal excited in resonance with optical transitions $(1/2; -3/2)$ (red curve) and $(-1/2; 3/2)$ (black curve). (c) Time dependence of the Kerr rotation signal amplitude. The straight lines are obtained using the exponential approximation of experimental data. The inset shows the lay out of experimental measurements of the Kerr rotation with temporal and spectral resolution. (d, e) The long-lived component of the Kerr rotation signal excited at the wavelength of the electronic transition to the lower (d) or upper (e) spin sublevel of the zero Landau level for the filling factor of a quantum Hall ferromagnet close to $\nu = 1$.

the ground state; see (8)) appears if the condition $\mathscr{L}k_{\text{photon}\,\parallel} \ll 1$ is fulfilled for the parallel plane of the system of the component of the wave vector of the absorbed photon. Here, $\mathscr{L}$ is the characteristic of spatial fluctuations of the electron density in the 2D ES. This condition is in fact fulfilled by a large margin. The elementary absorption process is one-photon and one-electron: after the fast 'vertical' recombination transition,[6] a 'spin-tilted' electron appears instead of the electron spin-polarized along the $\hat{z}$-axis:

$$|\nearrow\rangle = \begin{pmatrix} \cos\dfrac{\beta}{2} \\ -\sin\dfrac{\beta}{2} \end{pmatrix}.$$

At the same time, the indistinguishability of absorbed photons and the indistinguishability of electrons in 2D ESs pose the fundamental problem of the correct modeling of the quantum-mechanical state (8) (the determination of a set of coefficients $\{C_n\}$) adequately to the given method of creating a Goldstone mode. In fact, to study slow transverse relaxation (the precession rotation decay), it is sufficient to consider only the evolution of one of the basis states $|n\rangle$, because, as we will see, the relaxation decay is the same for all terms in sum (8). In addition, as was mentioned, for a macroscopic mode, only a small vicinity of states near a value n_0 ($|n - n_0| \ll n_0$) specified by the macroscopic parameter $|S_\perp|$ or θ is important.

Before proceeding to the solution of the microscopic relaxation problem, it is necessary to elucidate the physical meaning of the quantity N in sum (8). Note that the operator $\hat{S}_-$ acting on $|0\rangle$ flips the spin of one electron, leading to the result corresponding to the indistinguishability principle. The correct normalized state of a system with one electron spin flip has the form $\mathcal{N}_\phi^{-1/2}\hat{S}_-|0\rangle \equiv \mathcal{N}_\phi^{-1/2}|1\rangle$. The state of one electron with the 'tilted' spin can be represented as a combination of the spin up and spin down states,

$$|\nearrow\rangle = \cos\frac{\beta}{2}|\uparrow\rangle - \sin\frac{\beta}{2}|\downarrow\rangle.$$

Therefore, the correct normalized state of the total multi-electron system with one 'spin-inclined' electron is the combination

$$\cos\frac{\beta}{2}|0\rangle - \sin\frac{\beta}{2}\,\mathcal{N}_\phi^{-1/2}|1\rangle.$$

In this state, as it should be, the probability of the spin projection S_z having the value $\mathcal{N}_\phi/2$ is $\cos^2(\beta/2)$, the probability of having the value $\mathcal{N}_\phi/2 - 1$ is $\sin^2(\beta/2)$, but the probability of having a value smaller than $\mathcal{N}_\phi/2 - 1$ is identically zero. It is clear that, if a system contains not one but N 'spin-tilted' electrons, then the nonzero probability should always exist for the projection S_z to have the value $\mathcal{N}_\phi/2 - N$, but the probability of having any smaller value is strictly zero. It follows that the number N of the leading term in the expansion is nothing but the number of 'spin-tilted' electrons. Or, in other words, this is the number of efficiently absorbed photons, so that, as a result, N electrons from the total number $\mathcal{N}_\phi$ pass from the $|\uparrow\rangle$ state to the $|\nearrow\rangle$ state. The relation of the number N to the deviation angle θ is determined from simple geometrical considerations: because the mean value of the spin projection on the $\hat{z}$-axis of each of the 'spin-tilted' electrons is $(1/2)\cos\beta$, the mean value of the projection of all $\mathcal{N}_\phi$ electrons is

$$\langle S_z\rangle = \frac{\mathcal{N}_\phi - N}{2} + \frac{N}{2}\cos\beta.$$

This gives

$$\cos\theta = \frac{2\langle S_z\rangle}{\mathcal{N}_\phi} \equiv 1 - \frac{2N}{\mathcal{N}_\phi}\sin^2\frac{\beta}{2}.$$

The number N is determined by the optical pulse power, i.e., the deviation angle depends both on the angle of incidence β of the laser beam and on the laser pump power. The rotation of all spins as a whole would correspond only to a particular case when $N = \mathcal{N}_\phi$.

Finally, we will study the slow evolution of a Goldstone mode that occurs with perturbations acting on spins taken into account. Consider one of the stationary states $|n\rangle$, which is also an eigenstate for spin operators $\hat{\mathbf{S}}^2$ and $\hat{S}_z$. This condensate of n Goldstone excitons can be destroyed not only in processes changing the total number of magnetoexcitons [see (10)] but also in a simpler one-exciton transition $n\mathrm{X_G} \to (n-1)\,\mathrm{X_G} + \mathrm{X}_\mathbf{q}$, when the Goldstone exciton transforms into a spin-wave exciton. In this case, the total number of magnetoexcitons is conserved and, therefore, the value of S_z is conserved. The perturbation responsible for this transformation (i.e., in fact, for the elementary process $\mathrm{X_G} \to \mathrm{X}_\mathbf{q}$) conserving the projection S_z should not conserve the total spin, which decreases by unity according to the above discussion of the spin numbers of the Goldstone and spin-wave excitons. In addition, this perturbation should break the spatial translation symmetry and lead to the appearance of a nonzero momentum $\mathbf{q}$ in the system. All these conditions correspond to the spatial fluctuations of the g-factor in 2D ESs: $g = \langle g\rangle_R + g_1(\mathbf{r})$, i.e., now the term

$$\hat{V}_g = \frac{1}{2}\,\mu_\mathrm{B} B \sum_i g_1(\mathbf{r}_i)\,\sigma_{zi}$$

is added to the Zeeman interaction operator, where i is the electron number and σ_{zi} is the Pauli operator acting on the spin of the ith electron. The kinetic approach to the solution to the problem involves the transition from the state $|1\rangle = \hat{S}_-|0\rangle$ to the state $|f_\mathbf{q}\rangle = \mathcal{Q}_\mathbf{q}^\dagger|0\rangle$, where $\mathcal{Q}_\mathbf{q}^\dagger$ is the spin-wave exciton creation operator (see [12, 13, 56, 76] and references therein). Here, we will not consider in detail routine quantum-mechanical calculations performed by the exciton representation method.[7] The general scheme, as usual, requires the calculation of the matrix element $\mathcal{M}_{f_\mathbf{q}} = \langle 1|\hat{V}_g|f_\mathbf{q}\rangle$ and then the transition time

$$\frac{1}{\tau} = \frac{2\pi}{\hbar}\sum_\mathbf{q} |\mathcal{M}_{f_\mathbf{q}}|^2\delta(\epsilon_\mathrm{Z} - E_\mathbf{q}). \tag{11}$$

[6] The photon absorption process is mainly reduced to the 'gemini' recombination at which a photon-created pair consisting of an electron and a heavy valence hole is annihilated before quasi-particles are separated by a distance exceeding the scale of their wave functions. However, a recombination channel also exists in which a hole is annihilated (due to the radiative transition) not with its 'own' electron created simultaneously with the hole but with an electron from the conduction band located in the hole's 'quantum vicinity'. In this case, its 'own' electron having an 'tilted' spin ($\nearrow$) due to the conservation of the total angular momentum will occupy a vacancy produced at the Landau level in the conduction band. In this way, the $|\uparrow\rangle \to |\nearrow\rangle$ transformation is realized. Recombination transitions take place simultaneously with fast nonradiative processes. In particular, the fast spin relaxation of the created valence hole occurs.

[7] The substantiation of the kinetic approach based on the general representation for the Goldstone mode (8) and calculations of the transformation time of the Goldstone exciton to a spin-wave exciton will be published later [94].

Here, the spin-wave exciton energy $E_{\mathbf{q}}$ is determined by expression (4), where we can pass to the limit $\mathscr{E} \to 0$ in the principal approximation. The characteristic destruction time of a condensate of Goldstone excitons can be estimated by introducing the correlator $K(\mathbf{r}) = \langle g_1(\mathbf{R})\, g_1(\mathbf{R}+\mathbf{r})\rangle_R$ parametrized by the fluctuation amplitude Δ_g and the correlation length Λ_g. Assuming, as for a smooth random potential, that this correlator is Gaussian, $K(\mathbf{r}) = \Delta_g^2 \exp(-r^2/\Lambda_g^2)$, we find

$$\frac{1}{\tau} = \frac{\pi M_{\mathrm{X}}}{\hbar}\left(\frac{\mu_{\mathrm{B}} B \Lambda_g \Delta_g}{2 l_B}\right)^2 . \tag{12}$$

Microscopically, this result gives the characteristic destruction time for each of the Goldstone condensates $|n\rangle$ independent of n. This time can be called the dephasing time or the stochastization time of the coherent precession rotation, because the effect is related to the fact that the precession of individual spins in different regions of the 2D space occurs at a frequency somewhat different from the Larmor frequency $\epsilon_{\mathrm{Z}}/\hbar$.

Note that the mass M_{X} of a spin-wave exciton is the only physical quantity responsible for the multiparticle Coulomb interaction (the stronger the Coulomb coupling, the smaller the mass of the spin-wave exciton). Thus, the exchange 'consolidation' of electrons in a quantum Hall ferromagnet prevents the stochastization of precession: the time increases upon increasing the Coulomb coupling.

We can assume that spatial fluctuations of the g factor reflect in some way the spatial disorder of the smooth electrostatic potential and, therefore, set $\Lambda_g = \Lambda \sim 50$ nm for the estimate. As for the amplitude Δ_g, its ratio to the vacuum value $g_0 = 2$ should be of the order of the ratio of the amplitude Δ to the bandgap. Assuming $\Delta_g \simeq 0.005$, which seems realistic, we can estimate the Goldstone exciton stochastization time as $\tau \sim 1-10$ ns ($M_{\mathrm{X}}^{-1} \sim 2$ meV in the field $B \approx 3-10$ T).

The macroscopic stochastization picture is as follows. The mean quantum-mechanical value of the longitudinal component S_z is invariable. The considered process corresponds to the change in the transverse component $S_\perp(t)$ of the total spin, which follows at small deviations ($|S_\perp(0)| \ll \mathcal{N}_\phi/2$) the equation $\mathrm{d}|S_\perp|/\mathrm{d}t = -|S_\perp|/\tau$, i.e., decays exponentially as $|S_\perp| = |S_\perp(0)| \exp(-t/\tau)$ (large deviations would mean that the concentration of magnetoexcitons is high, $n \sim \mathcal{N}_\phi/2$, i.e., the number of spin-wave excitons also becomes large for $t \gtrsim \tau$, and their interaction with each other proves to be significant, which, of course, was ignored here). The estimated time $\tau \sim 1-10$ ns corresponds, according to the generally accepted terminology, to the spin transverse relaxation time T_2. In turn, the longitudinal relaxation process describing the relaxation of S_z to its equilibrium value was considered in Section 3. The theoretical and experimental values of the longitudinal time prove to be considerably longer: $T_1 \sim 100$ ns. Note that the relation $T_2 \ll T_1$ is also valid for spin relaxation in classical exchange ferromagnets. At the same time, the theory of transverse relaxation in 2D ESs presented here is not related to any previously described mechanism.

Direct measurements of the precession stochastization time were performed with high-quality $\mathrm{GaAs/Al}_x\mathrm{Ga}_{1-x}\mathrm{As}$ heterostructures with single QWs containing highly mobile 2D ESs ($\mu_{\mathrm{e}} \simeq 5 \times 10^6$ cm^2 V^{-1} s^{-1}) with concentrations $n_{\mathrm{e}} \simeq 0.7 \times 10^{11}$ cm^{-2} (sample A) and $n_{\mathrm{e}} \simeq 2.4 \times 10^{11}$ cm^{-2} (sample B). A Kerr rotation signal was excited by a tunable picosecond Ti:sapphire laser. The mean excitation power did not exceed $\simeq 1$ mW. The laser beam spot diameter was 1 mm. The circularly polarized pump pulse specified the orientation of the spin of the excited 2D ES. The rotation angle of the polarization plane was measured with the help of a linearly polarized probe beam reflected from the sample. Measurements were performed in the degenerate regime when the pump laser wavelength coincided with the probe radiation wavelength. Samples were placed in an optical cryostat with a superconducting solenoid at an angle of 45° with respect to the magnetic field direction. The excited electron spins were oriented approximately normally to the sample surface because of a large difference between the refractive indices of GaAs and liquid helium. The experimental setup reproduced that used in [8, 9]. The difference was that the spectral width of our excitation source was smaller (0.7 meV). This allowed us, by varying the pump wavelength, to change upon excitation the proportions of optical transitions into two different spin states of the zero Landau level (i.e., thereby changing the effective angle between excited spins and the magnetic field). The generated spin excitations had zero transverse (along the QW plane) momentum because of the reflection geometry used. Thus, excitation generated mainly Goldstone excitons.

The decay of the beat amplitude of the Kerr rotation signal (the difference between the signal maximum and minimum) is divided into two time intervals (Figs 7b, c): the short interval $T_{\mathrm{S1}}^{\mathrm{e}}$ (a few hundred picoseconds) and long interval $T_{\mathrm{S2}}^{\mathrm{e}}$ (a few nanoseconds). In addition, the beat signal is modulated by long-term oscillations observed in samples with the highest mobility (Figs 7d, e). We assign long-term oscillations to the collective degrees of freedom of the total electron system, whose nature is still unknown. The relaxation time $T_{\mathrm{S1}}^{\mathrm{e}}$ is independent of the filling factor, while the dependence of $T_{\mathrm{S2}}^{\mathrm{e}}$ on the filling factor becomes essentially nonmonotonic near quantum Hall ferromagnetic states with filling factors $\nu = 1$ and $\nu = 3$. Since the initial phase relaxation ($T_{\mathrm{S1}}^{\mathrm{e}}$) is not related to the filling factor, it is explained by one-electron spin relaxation. The electron system is overheated after the pump pulse and the relaxation time $T_{\mathrm{S1}}^{\mathrm{e}}$ appears due to the fast cooling of the electron system [74]. This assumption is confirmed by the fact that the increase in the pump power increases the proportion of states relaxing with the time $T_{\mathrm{S1}}^{\mathrm{e}}$ in the Kerr rotation signal. Below, we will consider the long relaxation channel ($T_{\mathrm{S2}}^{\mathrm{e}}$) sensitive to the spin ordering of the ground state.

The transverse spin relaxation times measured in a quantum Hall ferromagnet ($\nu = 1$) agree well with the stochastization times of Goldstone spin excitons estimated theoretically above for high-mobility $\mathrm{GaAs/Al}_x\mathrm{Ga}_{1-x}\mathrm{As}$ heterostructures. In addition, it was found that spin relaxation times in the vicinity of values $\nu = 1$ and $\nu = 3$ changed nonmonotonically and more than an order of magnitude (Fig. 8). Such a great variation in the spin relaxation time is perfectly consistent with the result of Ref. [95] about the influence of the spin transformation in a quantum Hall ferromagnet on the nuclear spin relaxation time. This effect is explained by the following reason. When the electron system undergoes a quantum phase transition from a quantum Hall ferromagnetic state to a less rigid spin ordering (spin-texture liquid or a skyrmion crystal), new phase-destruction mechanisms of the coherent spin precession begin to play a role due to the appearance of spin excitations with an energy smaller than the Zeeman energy

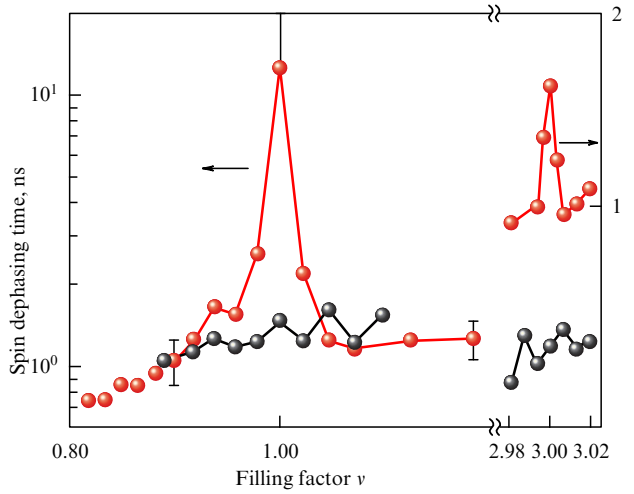

Figure 8. (Color online.) Decay time of the long-lived component of the Kerr rotation signal measured upon excitation at the wavelength of the electronic transition to the lower (red circles) or upper (black circles) spin sublevels of the partially filled Landau level for filling factors close to $\nu = 1$ (total magnetic field is $B = 4.50$ T, sample A) and $\nu = 3$ ($B = 4.65$ T, sample B).

[88, 89]. Spin relaxation times also decrease on passing from a more 'rigid' (strong exchange interaction between electrons) quantum Hall ferromagnetic state with $\nu = 1$ to a softer (weak exchange interaction) quantum Hall ferromagnetic with state $\nu = 3$.

5. Spin relaxation in a quantum Hall insulator with the electron filling factor $\nu = 2$

As mentioned in the Introduction, the lowest-energy collective electronic excitations in a quantum Hall insulator with $\nu = 2$ are magnetoexcitons formed by an excited electron at the unfilled first Landau level and a Fermi hole (electron vacancy) at the completely filled zero Landau level (Fig. 9a). In other words, this is a cyclotron magnetoplasmon with zero spin ($S = 0$) or a spin-cyclotron triplet exciton with unity total spin ($S = 1$). The radiative lifetime of a magnetoplasmon is determined by the dipole-allowed electron recombination from the first Landau level ($n_L^e = 1$) with emission of a photon with an energy equal to the cyclotron energy. The characteristic recombination time is about 1 ns [96]. Unlike magnetoplasmons, spin-cyclotron excitons are 'dark', their radiative annihilation being strictly forbidden due to spin conservation.

The energy of all three components of a spin-cyclotron exciton in GaAs/$Al_xGa_{1-x}As$ structures is lower than the magnetoplasmon energy for any value of the momentum, including the particular case of $q = 0$ [30, 31]. These components are always equidistantly separated by the Zeeman gap ϵ_Z. In other words, the energy of triplet components is described by the expression

$$E_t = \hbar\omega_c - \epsilon_Z S_z + \mathscr{E}_q$$

(the negative value of the Lande g-factor is taken into account), where $\mathscr{E}_q$ is the part of energy determined by the Coulomb interaction. In the ultra-two-dimensional case in the first approximation in the interaction, this quantity was calculated in [29]. Taking into account a finite width of QWs,

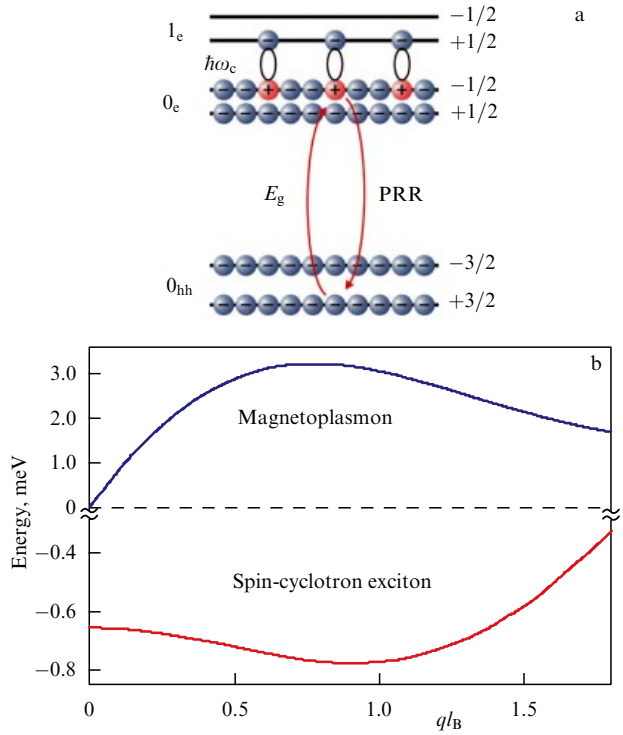

Figure 9. (Color online.) (a) Diagram of one-electron states of a quantum Hall insulator ($\nu = 2$) upon excitation of a triplet spin-cyclotron exciton. In the left part of the figure the numbers of Landau levels are indicated for an electron in the conduction band (0_e, 1_e) and a heavy hole in the valence band (0_{hh}); in the right part the values of the spin projection are indicated S_z. The excited electron undergoes transition from the lowest completely filled Landau level ($n_L^e = 0$) to the nearest empty cyclotron level ($n_L^e = 1$) occupying its lower spin sublevel in the spin-flip state. This electron is coupled with a positively charged Fermi hole at the upper spin sublevel of the zero Landau level ($n_L^e = 0$) to form a triplet state (schematically shown by ellipses). The bent arrows illustrate the virtual absorption and reemission of a photon during PRR recording. E_g is the bandgap and $\hbar\omega_c$ is the cyclotron energy. (b) Dispersion dependences of two-particle excitations in a QW 32 nm wide in a 4.2-T magnetic field calculated for a spin-cyclotron exciton (red curve) and a magnetoplasmon (blue curve) (see explanations in the text).

in the first approximation in the dimensionless parameter $r_s = e^2/(\kappa l_B \hbar\omega_c)$, this energy is $\hbar\omega_c r_s \varepsilon_1(q)$, where

$$\varepsilon_1(q) = \int_0^\infty \mathrm{d}s \exp\left(-\frac{s^2}{2}\right)\mathcal{F}(s)\left(1 - \frac{s^2}{2}\right)\left[1 - J_0(sql_B)\right],$$

J_0 is the Bessel function, and $\mathcal{F}(s)$ is the form factor depending on the size quantization wave function $\chi(z)$ of an electron in the QW,

$$\mathcal{F}(s) = \iint \mathrm{d}z_1\,\mathrm{d}z_2 \exp\left(\frac{-s|z_1 - z_2|}{l_B}\right)\left|\chi(z_1)\chi(z_2)\right|^2. \quad (13)$$

In addition, because ε_1 vanishes for $q = 0$, the second-order correction in r_s becomes essential for small values of the wave vector ($ql_B \ll 1$), i.e.,

$$\mathscr{E}_q \approx \hbar\omega_c\left(r_s\varepsilon_1(q) + r_s^2\varepsilon_2(q)\right).$$

The function $\varepsilon_2(q)$ does not vanish for $q \to 0$. On the contrary, this function determines the negative Coulomb shift of the triplet observed in Raman spectra [30]. This

quantity was calculated in [31]:

$$\varepsilon_2(0) = -\sum_{n=2}^{\infty} \frac{2-2^{2-n}}{nn!(n^2-1)} \int_0^{\infty} \mathrm{d}s\, s^{2n+1} \mathcal{F}^2(s) \exp(-s^2)$$

(in the ultra-two-dimensional case when $\mathcal{F}(s) = 1$, we find $\varepsilon_2(0) = (\ln 2 - 1)/2 = -0.1534...$). A specific calculation shows that the first-order correction ($\propto \varepsilon_1$), which is negative for $ql_B \lesssim 1$, is quite numerically small even for $ql_B \sim 1$. As a result, for all the actual values of $ql_B \lesssim 1$, the second-order correction that makes a considerable contribution to the total Coulomb shift should be taken into account. By simply extrapolating the principal approximation (for conditionally small parameters r_s and ql_B) and estimating the Coulomb energy depending on q as

$$\mathscr{E}_q = \frac{e^2}{\kappa l_B} \varepsilon_1(ql_B) + 2\mathrm{Ry}\, \varepsilon_2(0)$$

(here, $2\mathrm{Ry} = (e^2/\varepsilon l_B)^2/(\hbar\omega_c) = m_e^* e^4/(\varepsilon^2\hbar^2)$), we obtain the total negative shift of a spin-cyclotron exciton with respect to the level $\hbar\omega_c$ consisting of the Zeeman and Coulomb parts $-\epsilon_Z + \mathscr{E}_q$. This quantity calculated for a particular QW is shown in Fig. 9b (red curve). For comparison, the figure also shows the 'positive' spectrum of a magnetoplasma wave (blue curve), which is determined only by the Coulomb interaction of electrons.

The authors of this review developed experimental methods [32] for exciting an ensemble of translation-invariant spin-cyclotron excitons with $S_z = +1$, controlling its parameters and studying the kinetics of relaxation of these excitations to the ground state by using the resonance reflection of light for optical transitions across the bandgap. A priori, we can assume that, upon testing a quantum Hall insulator with the filling factor $\nu = 2$, the resonance reflection signal corresponding to the transition from the zero Landau level of heavy holes in the valence band ($n_L^h = 0$) to the zero Landau level of electrons in the conduction band ($n_L^e = 0$) should be absent, because all the electronic states of the ground electronic cyclotron level are completely filled. However, with optical pumping, at which excited electrons undergo transitions to the upper Landau levels ($n_L^e \geqslant 1$), it is reasonable to expect at a low enough temperature the formation of these lowest-energy excitations with $S_z = +1$ (hereafter, we will call them simply spin-cyclotron excitons).

The formation of spin-cyclotron excitons should be manifested in a decrease in the number of unfilled states of the first electronic Landau level ($n_L^e = 1$) and in the simultaneous appearance of the Fermi-hole states at the zero electronic level ($n_L^e = 0$). It is reasonable to call the corresponding changes in resonance reflection spectra photoinduced resonance reflection (PRR).

PRR spectra should exhibit two peaks: a positive one corresponding to the optical transition from the zero cyclotron level of heavy holes ($n_L^h = 0$) to the upper spin sublevel of the zero cyclotron level of 2D electrons ($n_L^e = 0$) (the 0–0 transition) and a negative peak corresponding to the transition from the first cyclotron level of heavy holes of the valence band ($n_L^h = 1$) to the first electronic cyclotron level ($n_L^e = 1$) (the 1–1 transition). While the positive peak is responsible for the appearance of Fermi holes on the upper spin sublevel of the zero cyclotron level of electrons ($n_L^e = 0$), the negative peak is responsible for the decrease in the number of vacancies at the first cyclotron electronic level ($n_L^e = 1$). Thus, the PRR method allows us to test indirectly optically inactive spin-cyclotron excitons using optically allowed resonance transitions between the discrete Landau levels of heavy holes of the valence band and the discrete Landau levels of electrons in the conduction band.

In [32], high-quality $GaAs/Al_xGa_{1-x}As$ heterostructures with the dark mobility of 2D electrons in the range of $(5-20)\times 10^6\ \mathrm{cm^2\ V^{-1}\ s^{-1}}$ were used. The high quality of the structures is extremely important for observing spin-cyclotron excitons. Experiments were performed with two sets of samples with single $GaAs/Al_xGa_{1-x}As$ QWs 17 and 35 nm wide symmetrically doped on both sides. The QW width in each set remained fixed, while the electron concentration in the 2D channel in different samples was varied in the range of $5\times 10^{10} - 2.5\times 10^{11}\ \mathrm{cm^{-2}}$. Experiments with an individual sample with a certain electron concentration provided the measurement of one point on the experimental plot of the dependence of the spin relaxation on the magnetic field for the fixed filling factor $\nu = 2$ (one experimental point — one sample).

Samples with a characteristic size of 3×3 mm were placed into a liquid ^{3}He cryostat equipped with a helium vapor pumping system. This cryostat was placed, in turn, into a liquid ^{4}He cryostat with a superconducting solenoid. Such a cryosystem provided optical and transport measurements at temperatures down to 0.45 K in a magnetic field up to 14 T. Spectral measurements were performed using two multimode fused silica fibers 400 μm in diameter and having a 0.39 numerical aperture. One fiber was used to deliver laser radiation to a sample, and the other to collect the light signal from the sample and to deliver it to the entrance slit of a diffraction spectrometer equipped with a cooled CCD camera. Resonance reflection measurements were performed with the fibers mounted symmetrically at an angle of $\approx 10^\circ$ to the sample normal, so that the central axis of a laser beam reflected from the sample coincided with the receiving fiber axis. The laser light scattered and reflected from the surfaces of the sample and fibers was suppressed with crossed linear polarizers mounted between the ends of the fibers and the sample.

In [32], two tunable cw lasers were used, one of them for the resonance excitation of a 2D electron system and the other for measuring the PRR, PL, and inelastic light scattering (ILS) spectra. To avoid the overheating of samples, the laser pump exciting electrons to high Landau levels with quantum numbers $n_L^e \geqslant 1$ did not exceed 0.3 mW. The probe laser power introduced to the same fiber was an order of magnitude lower. Resonance reflection spectra were measured by scanning a probe laser and detecting the laser line intensity with a CCD camera at the spectrometer exit. The differential PRR spectrum was obtained as the difference between resonance reflection spectra obtained with and without laser pumping.

The PRR spectra were used to control the creation of photoexcited electrons at the first electronic level ($n_L^e = 1$) and Fermi holes at the zero level ($n_L^e = 0$). The PRR spectrum exhibits, as predicted, a positive peak in the 0–0 transition region and a negative peak in the 1–1 transition region (Fig. 10). This is caused by the formation of low-energy magnetoexcitons consisting of electrons at the first Landau level coupled with the Fermi holes of the zero electronic level.

Although spin-cyclotron excitons are optically inactive, they can be found directly from ILS spectra (see the inset in Fig. 10) and then used for determining the singlet-triplet

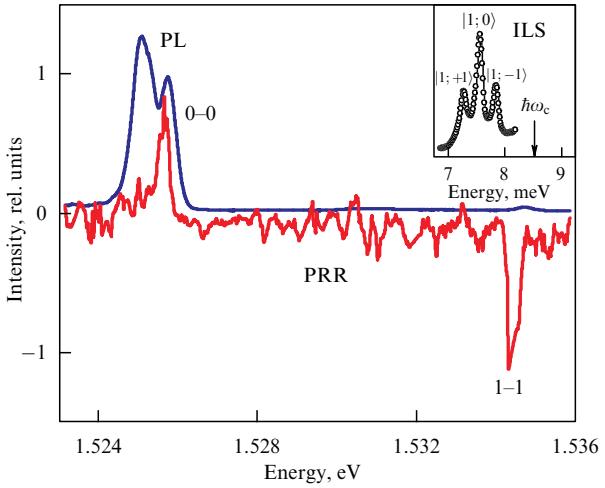

Figure 10. PL and PRR spectra for $\nu = 2$ measured in a GaAs/$Al_xGa_{1-x}As$ QW 17 nm wide ($\mu_e = 5 \times 10^6$ cm^2 V^{-1} s^{-1}, $n_e = 2.4 \times 10^{11}$ cm^{-2}) in a 5-T magnetic field at temperature $T = 0.45$ K. The 0–0 optical transition occurs between the ground levels of electrons in the conduction band ($n_L^e = 0$) and of heavy holes in the valence band ($n_L^h = 0$), while the 1–1 transition occurs between the first cyclotron levels $n_L^e = 1$ and $n_L^h = 1$. The PL spectrum exhibits a circularly polarized doublet (σ^+- and σ^--components), corresponding to 0–0 electronic transitions. The doublet splitting is exactly equal to the sum of the spin splitting of the ground cyclotron level of heavy holes in the valence band in a magnetic field ($n_L^h = 0$) and the spin splitting of the ground cyclotron level of 2D electrons in the conduction band ($n_L^e = 0$). The inset shows the resonance ILS spectrum measured under the same experimental conditions and the parallel component of the 5-T magnetic field introduced to increase the Zeeman splitting of components of the spin-cyclotron triplet.

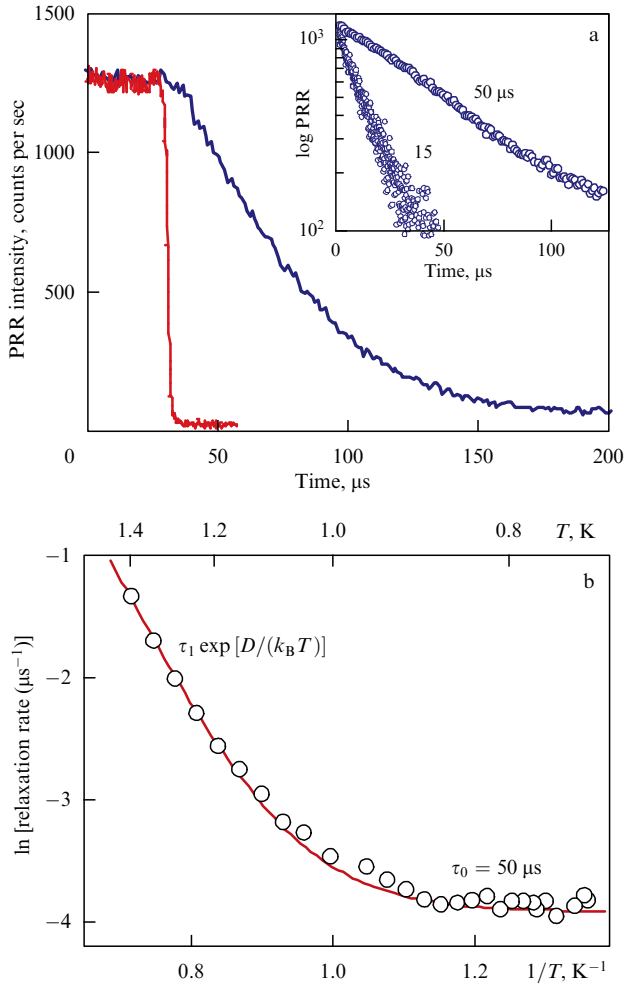

Figure 11. (Color online.) (a) PRR decay kinetics (blue curve) and, for comparison, the instrument function of the measurement system (red curve). The inset shows on a semi-logarithmic scale the decay kinetics measured for a QW 35 nm wide (long-time kinetics) and 17 nm wide (short-time kinetics) for $\nu = 2$ in a perpendicular 4-T magnetic field. In both QWs, $n_e = 2 \times 10^{11}$ cm^{-2}, and $\mu_e = 1.5 \times 10^7$ cm^2 B^{-1} s^{-1} and 5×10^6 cm^2 B^{-1} s^{-1}, respectively. (b) Temperature dependence of the relaxation rate of spin-cyclotron excitons on the logarithmic scale in a QW 35 nm wide in a 4-T magnetic field. Circles are experimental data; the curve is an approximation taking into account the activation and temperature-independent relaxation mechanisms.

splitting of magnetoexcitons for the zero wave vector [30]. The singlet-triplet splitting is measured as the difference between the magetoplasmon energy and 'the center of gravity' of the triplet (positions of components with $S = 1$ and $S_z = 0$ in the spectrum). This splitting proved to be comparatively large, about 1 meV [32], which may seem strange, because the singlet-triplet splitting in bulk GaAs crystals is very small, only ≈ 20 μeV [97, 98].

However, first, one should take into account that matrix elements of the exchange interband Coulomb interaction are suppressed compared to these for the intraband exchange due to the difference between electronic Bloch functions in different bands. Second, in the presence of spatial restrictions reducing the system dimension (quantum confinement), the singlet-triplet splitting considerably increases due to an increase in the exchange electron-hole interaction. Thus, for example, this spitting in quite narrow GaAs QWs already reaches about 150 μeV [97]. In the case of 2D spin-cyclotron excitons in a quantum Hall insulator considered here, a transverse magnetic field (up to 10 T) provides a strong spatial restriction for carriers resulting in a considerable increase in the singlet-triplet splitting, up to approximately 1 meV.

The PRR kinetics were measured by modulating the laser pump radiation with a mechanical chopper — a rotating disc with a radial slit. For a disc rotation period of ≈ 11 ms and laser spot focusing on the disc with a microscope objective, the duration of the front (decay) of the formed laser pump pulse was ≈ 2 μs for a total pulse duration of $\leqslant 3$ ms. The probe laser wavelength was tuned to the maximum (minimum) in the PRR spectrum for recording the signal decay (rise) after the pump pulse ended. The testing laser radiation reflected from the sample surface was transmitted through a narrowband interference filter (bandwidth of ≈ 1.1 nm) to reject the pump radiation and then was focused on a silicon avalanche photodiode operating in the photon counting regime. The resonance reflection signal was measured with a gated photon counting system and was accumulated as a function of the time delay after switching off the exciting laser pulse. As a result, the PRR decay (or rise) curve was recorded.

The behavior of the nonradiative lifetime of spin-cyclotron excitons, which is directly related to the spin relaxation, was studied as a function of temperature and a magnetic field in QWs with various widths. For this, the PRR kinetics were studied upon pulsed laser excitation. The decay of PRR signals was found to be exponential with decay times (spin relaxation times) reaching several tens or even hundreds of microseconds (Fig. 11a). The PRR signal rise kinetics in the 1–1 transition region proceed at the same time scales, which indicates the common relaxation dynamics of magnetoexci-

ton states formed from electrons at the first Landau level and Fermi holes at the zero electronic Landau level. This commonality is also manifested in the same temperature dependence of the relaxation rate (Fig. 11b). For $T > 1$ K, the temperature dependence of the relaxation rate is exponential, $1/\tau(T) = \exp(-D/T)/\tau_1$ with the characteristic time $\tau_1 \approx 1$ ns and the activation bandgap $D \approx 11$ K.

Such a behavior suggests that in this temperature region the activation relaxation channel operates, which includes comparatively slow electron spin-flip processes caused by spin-orbit interaction and an increase in the excitation energy up to the cyclotron energy due to phonon absorption, followed by rapid relaxation due to photon emission with the cyclotron energy [15]. Under such conditions, the measured activation gap D is nothing but the binding energy of a spin-cyclotron exciton equal to the sum of the Zeeman energy and the Coulomb energy of the spin-cyclotron splitting, i.e., to $\epsilon_Z + |\mathscr{E}_{q_m}|$, where $q_m \simeq 1/l_B$ (Fig. 9b). This energy measured independently from ILS spectra is close to the activation gap.

In the low-temperature region $T < 0.8$ K, the PRR kinetics become temperature-independent. Therefore, in this temperature region, the relaxation mechanism changes, and this mechanism is no longer thermally activated. It is assumed that in the low-temperature region the nonradiative relaxation of a spin-cyclotron exciton occurs, followed by the creation of short-wavelength acoustic phonons receiving the exciton energy. This decay mechanism was earlier proposed and analyzed in [15]. The theory predicts, in particular, that the relaxation time τ_0 in this case should superlinearly depend on the electron wave function extension in the QW growth direction.

To verify this prediction, we studied two QWs with widths of 17 and 35 nm and approximately equal 2D electron concentrations. The half-widths of the envelopes of the electron wave functions in these QWs differed by approximately two times. Experimental results qualitatively confirm the theoretical prediction: (1) the relaxation time increases in the wider QW because it is more difficult to break the translation symmetry in the growth direction in the wide QW; (2) the relaxation rate decreases with increasing magnetic field because the electron–phonon interaction for higher-frequency acoustic phonons with frequencies close to the cyclotron frequency considerably weakens. We conclude that the qualitative agreement between experiments and the theoretical relaxation mechanism is good as a whole; however, the theory predicts longer relaxation times than the experimental values.

Thus, direct measurements of the PRR kinetics have shown that at low temperatures $T \ll T_{ST}$ ($k_B T_{ST}$ is the spin-cyclotron splitting), the lifetimes of a spin-cyclotron exciton closely related to the spin relaxation of the entire electron system are unusually long, amounting to a few hundred microseconds. Due to such long lifetimes, it is possible to produce rather high densities of $\sim 10^{10}$ cm^{-2} of such photoexcited magnetoexcitons at relatively low optical pump powers, which do not cause the overheating of the electron system.

6. Condensate of two-dimensional fermions in a magnetic field

As mentioned in the Introduction, in a dense ensemble of spin-cyclotron excitons, the Bose–Einstein condensation phenomenon can be expected. It appeared that, with decreasing temperature, a phase transition having a number of unusual properties was really observed in an ensemble of dark triplet magnetoexcitons. The exciton relaxation time in the vicinity of the phase transition demonstrates a nonmonotonic behavior (Fig. 12b). The lifetime increases exponentially at temperatures down to 1 K and then decreases by half in a narrow temperature range from 0.7 to 0.8 K, which suggests a threshold decrease in the viscosity of the ensemble of spin-cyclotron excitons during their 'transport' from the excitation spot. This also reduces the lifetime of spin-cyclotron excitons directly in the laser spot. Such an assumption is natural, because it is difficult to imagine that such a small change in temperature, only 0.2 K, can so drastically change relaxation mechanisms. This assumption is analyzed in Section 8 and confirmed by direct measurements of the transport of spin-cyclotron excitons during this phase transition.

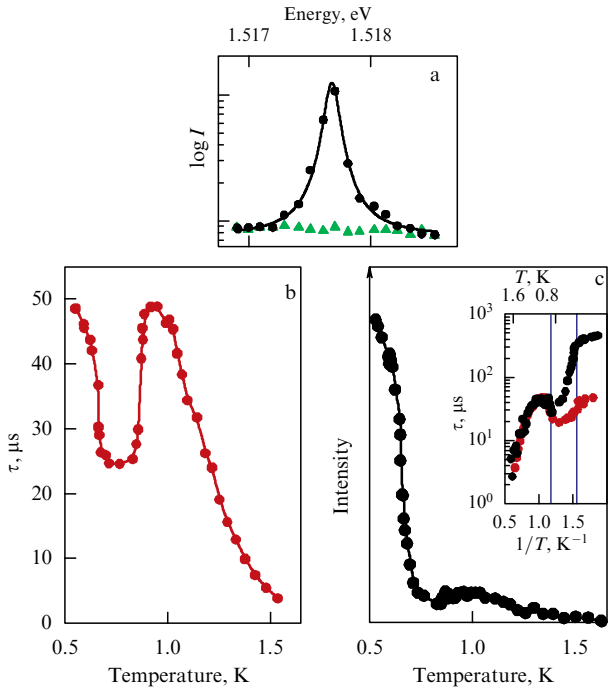

Figure 12. (Color online.) (a) Resonance reflection spectra of the equilibrium 2D ES (triangles) and a system disturbed from equilibrium by photoexcitation of an ensemble of spin-cyclotron excitons (dots). (b) Temperature dependence of the relaxation time of spin-cyclotron excitons upon stationary excitation of the 2D ES (dots). The solid curve is drawn for convenience. (c) Temperature dependence of the PRR signal intensity upon stationary photoexcitation of a 2D ES (dots). The inset compares the temperature dependences of the spin relaxation time of spin-cyclotron excitons (red dots) and the PRR intensity (black dots) measured at the same photoexcitation of the 2D ES. Here, the PRR intensity curve is multiplied by a constant to make both dependences coincide at $T > 1$.

It can be easily shown that the relaxation time $\tau(T)$ upon stationary photoexcitation is directly proportional to the exciton density $n(T)$: $\tau(T) \propto n(T)$. If the temperature dependence of the spin-cyclotron density is known, one can eliminate the density from the description of the response of the exciton ensemble to the resonance high-frequency electromagnetic field. By measuring the PRR signal $I(T)$ for the same photoexcitation level that was used to determine the relaxation time of a spin-cyclotron exciton ($I(T) \propto f(T)\,n(T)$, where $f(T)$ is the oscillator strength of the interband optical transition from the valence band to the

conduction band), we can obtain the dependence of the oscillator strength of the optical transition on the electron temperature: $f(T) \propto I(T)/\tau(T)$. Note that $f(T)$ is independent of temperature for $T > 0.8$ K, as expected for a system of magnetoexcitons with the Boltzmann energy distribution. However, as temperature further decreases, a giant threshold increase in the oscillator strength is observed (see the inset in Fig. 12c). We can conclude that, for the invariable exciton density, at the phase transition point the response of Fermi holes at the zero electronic Landau level involved in the spin-cyclotron exciton increases, which can be described in terms of exciton condensation.

Resonance reflection can be divided into two processes: resonance absorption and the subsequent photon emission with the transition of the system to the initial state. Therefore, it is sufficient to consider resonance absorption with the transition of the excited electron from the valence band to the conduction band to the vacancy appearing after creation of a spin-cyclotron exciton (to the Fermi hole at the zero Landau level). If the initial state of the ensemble of spin-cyclotron excitons follows the Boltzmann distribution and their number is considerably smaller than the number $\mathcal{N}_\phi$ of electronic states at the Landau level, it is easy to show that the square of the matrix element of the optical transition is proportional to $1/N_\phi$ and is independent of temperature. In the case of condensation of $1/N_\phi$ N spin-cyclotron excitons to the same quantum state, the square of the matrix element of the optical transition is proportional to N/N_ϕ [99].

The considerations presented above show that the square of the matrix element of the resonance absorption of electromagnetic radiation at the optical transition from the valence band to Fermi holes in the conduction band should increase proportionally to the number of spin-cyclotron excitons found in the same quantum state. The increase in the matrix element observed in experiments allows a conclusion that not all excitons are condensed to the same quantum state, and only a small number of them form coherent clusters of a finite size. By measuring the threshold temperature of the phase transition as a function of the photoexcitation intensity, we constructed the phase diagram for the condensation of spin-cyclotron excitons to the superabsorbing phase of such clusters in the pump intensity (or concentration)-temperature coordinates (Fig. 13).

Obviously, however, Fermi holes themselves contained in a spin-cyclotron exciton cannot be coherent in the sense that they are vacancies (empty sites) in the electron Fermi sea. In other words, it is not Fermi holes themselves that are coherent, but electrons separating them by forming a collective state (magnetofermion condensate), so that vacancies in this state behave coherently during interaction with the external electromagnetic field, providing, in turn, the superabsorption effect. This can mean that the theory considered in this section is only an approximate description of the properties of the nonequilibrium system discussed. Such a theory would be exact if the electron system under the Fermi level (electron vacuum) remained unperturbed after excitation of nonequlibrium excitons, which is equivalent to the replacement of the nonequilibrium electron system by an ensemble of spin-cyclotron excitons. By studying directly the properties of the electron vacuum, we show experimentally that such an assumption is, although reasonable, an inexact approximation to describe the properties of the nonequilibrium system considered.

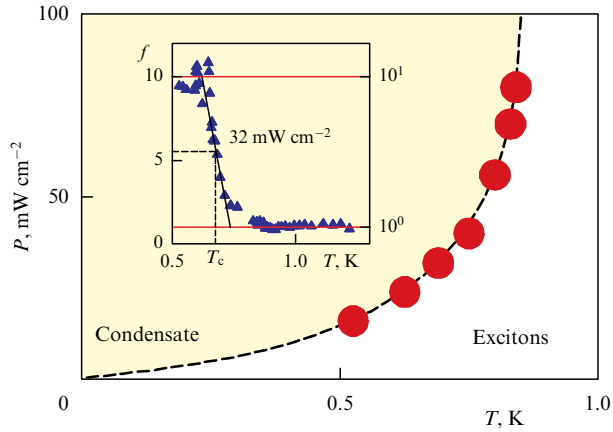

Figure 13. Phase boundary curve in the photoexcitation power density-temperature coordinates separating the regions of gas and a condensate of spin-cyclotron excitons (circles). The curve extended to the origin is drawn for convenience. The inset illustrates the determination of a point in the phase diagram by a change in the oscillator strength $f(T)$ of the optical transition from the valence band to the conduction band at a fixed photoexcitation level. The critical temperature T_c was chosen as a point at the half-height of the $f(T)$ increase step.

The response of an electron vacuum to external electromagnetic excitation was studied by the method of photoinduced PL, i.e., PL in the presence of a nonequilibrium ensemble of spin-cyclotron excitons. Unlike one optical transition in PRR, in photoinduced PL two optical transitions are possible: one of them is related to the recombination of an electron from the conduction band with a photoexcited hole from the valence band located far from the spin-cyclotron exciton (the influence of the exciton on the hole state in the valence band can be ignored), while the other is related to the recombination of an electron located in the immediate proximity to the spin-cyclotron exciton. The first recombination channel dominates at temperatures above 1 K. The second, nonequilibrium recombination channel begins to dominate in the PL spectrum when the electron system temperature is below the phase transition temperature. Here, it is reasonable to consider in more detail the properties of photoinduced PL for a small number of spin-cyclotron excitons.

7. Photoluminescence of electron-hole complexes in the presence of spin-cyclotron excitons

The photoluminescence of 2D ES in the presence of an ensemble of spin-cyclotron excitons is studied under resonance optical excitation, while the additional nonresonance pumping adds to the exciton ensemble high-energy e–h pairs consisting of an electron of the conduction band and a heavy hole in the QW valence band [100]. These pairs dissociate during relaxation and then return separately to the ground state. Depending on the number of additional high-energy pairs and density of spin-cyclotron excitons, some of the valence holes attach to excitons, forming positively charged three-particle complexes. The formation of negatively charged three-particle states is also possible, but such states are inactive in the experimentally accessible visible range and, therefore, they are not considered here. Thus, by changing the density of resonance and nonresonance excitations, it is

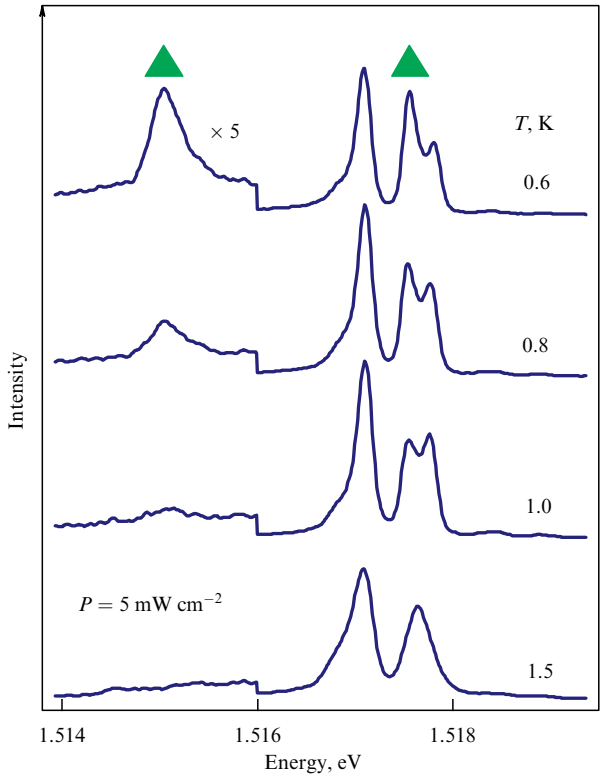

Figure 14. PL spectra at different temperatures for a pump power density of 5 mW cm^{-2}.

possible to create various stable complexes consisting of a spin-cyclotron exciton, electrons, and holes.

A system of long-lived spin-cyclotron excitons was created using two samples with symmetrically doped single $GaAs/Al_xGa_{1-x}As$ QWs 17 and 35 nm wide. At high enough temperatures (above 1 K), all excitons rapidly relax via the optical recombination channel. As a result, the interband recombination spectra of a valence hole and an electron from the filled Landau level exhibit only a circularly polarized ($\sigma^+ - \sigma^-$) Zeeman doublet corresponding to two dipole-allowed 0–0 optical transitions of electrons from the conduction band to the valence band of heavy holes (the lower spectrum in Fig. 14). The splitting of this doublet is exactly equal to the sum of spin splitting of heavy holes in the valence band and electrons in the conduction band. As temperature decreases, nonequilibrium spin-cyclotron excitons are accumulated in the 2D ES [32], and two additional lines appear in the PL spectrum.

Consider radiative recombination transitions from the zero Landau level of electrons in the conduction band to the zero Landau level of heavy holes of the valence band (Fig. 15). The spectrum of one-particle states is completely quantized; the Fermi level lies in the middle of the cyclotron gap between the zero and first Landau levels of electrons. For each of the two polarizations of the emitted photon, two transitions are allowed: the recombination transition in the absence of a spin-cyclotron exciton observed at higher temperatures and the transition between the inner states of a trion formed by the valence hole and the spin-cyclotron exciton. The latter transition is dipole-allowed when the inner quantum numbers of the trion do not change [101]. The final state of the second transition in the σ^- polarization is a trion formed by the excited electron and two Fermi holes at the zero Landau

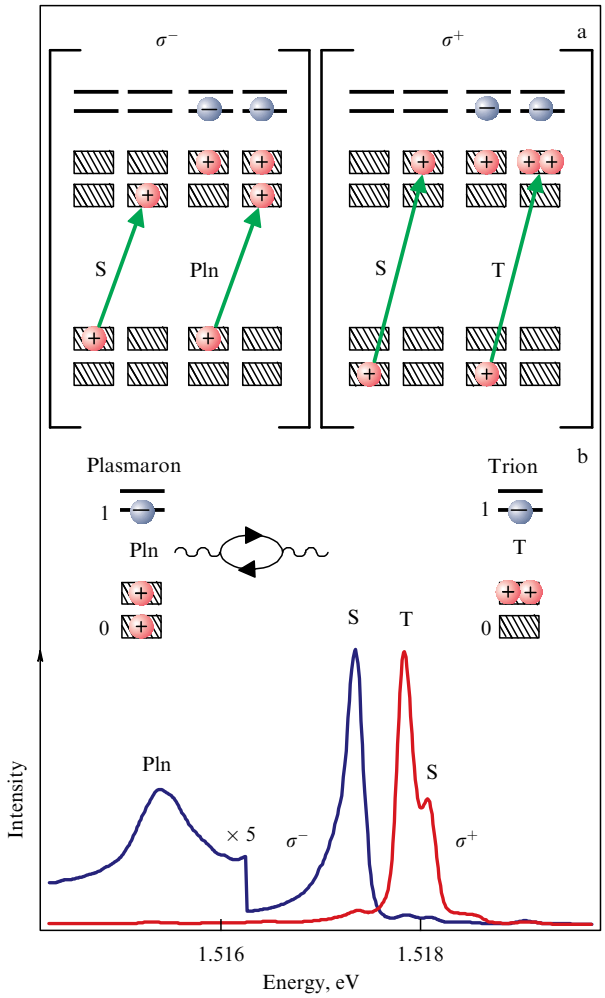

Figure 15. (Color online.) (a) Allowed optical transitions in σ^-- and σ^+-polarizations for one-particle states (S) and the three-particle state (Pln or T). (b) PL spectra for σ^- (blue) and σ^+ (red) polarizations in a QW 35 nm wide measured for $B = 4$ T and $T = 0.5$ K.

level in the conduction band with opposite spins (Pln). In the σ^+ polarization, this is a trion formed by the excited electron and two Fermi holes at the zero Landau level in the conduction band with parallel spins (the T state). In the T state, the excited electron from the first Landau level cannot occupy the site of the Fermi hole because of the conservation of the 2D ES spin. On the contrary, in the Pln state, the excited electron can occupy the site of one of the Fermi holes with emission of a cyclotron photon, which, in turn, can be absorbed with the creation of an e–h pair with the cyclotron energy, etc. If the system contained only one Fermi hole, the described process would correspond to excitation of a magnetoplasmon [29]. In the presence of the second Fermi hole, the three-particle Pln state is a *magnetoplasmaron*.

The energy of inner transitions for a T trion almost coincides with the energy of the one-particle transition at high temperatures. The 0.2-meV red shift is caused by the difference in the interaction of trion's particles during the transition of one of the holes from the valence band to the conduction band. The inner transition energy for the Pln trion leading to the formation of a magnetoplasmaron proves to be considerably smaller (by 2 meV) than the energy of the corresponding one-particle transition. Such a considerable

decrease in the energy is caused by plasma oscillations of a magnetoplasmaron.

The calculation of the manetoplasmaron energy is a complicated problem. To estimate the contribution of plasma oscillations to the energy, we consider a simplified model of transition from the initial two-particle state (a p-type magnetoexciton formed by a hole at the zero Landau level in the valence band and an electron at the first Landau level in the conduction band) to the final two-particle state (a magnetoplasmon with spin 0) by ignoring the Fermi hole in the conduction band entering into the composition of a spin-cyclotron exciton. The energy of the p-type magnetoexciton is minimal for the wave vector $q_{\mathrm{m}} \simeq 1/l_B$ (Fig. 9b). The contribution to the final state energy caused by plasma oscillations has the form

$$E_{\mathrm{MP}}(q_{\mathrm{m}}) = \frac{e^2}{\kappa}\, q_{\mathrm{m}} \mathcal{F}(q_{\mathrm{m}}) \exp\left[-\frac{(q_{\mathrm{m}} l_B)^2}{2}\right].$$

This expression, equal to the difference between the Coulomb energies of a magnetoplasmon and a spin-cyclotron exciton, agrees with the result obtained in [29], but taking into account the form factor $\mathcal{F}(q)$ (13). The measured magnetoplasmaron shift is smaller than the calculated energy $E_{\mathrm{MP}}(q_{\mathrm{m}})$. This discrepancy is not surprising, because calculations disregarded the influence of the third particle, the complicacy of the wave function of a hole in the valence band and also the possible influence of Coulomb corrections of second-order smallness in the Coulomb/cyclotron energy ratio [30].

The plasma nature of the Pln energy shift is confirmed by measurements performed for two QWs with different widths (Fig. 16): the decrease in the QW width increases the energy of plasma oscillations with changing $\mathcal{F}(q_{\mathrm{m}})$. The experimental magnetoplasmaron shift in the narrower QW is 1.4 times greater than that in the wide QW, which is consistent with the calculations presented above. The magnetoplasmaron shift measured in a broad range of electron densities also agrees with calculated values except the systematic shift to lower energies. The probability of magnetoplasmaron recombination increases upon increasing the number of spin-cyclotron excitons or additional e–h pairs. However, this recombination channel is saturated with increasing nonresonance pump power up to 7.5 mW cm^{-2}. As the nonresonance pump power was further increased, the magnetoplasmaron recombination line was quenched, and a new line appeared with the plasma shift exceeding that of the magnetoplasmaron line twofold.

A new Pln + E_{X} recombination line appears only in the σ^--polarization, corresponding to the transition of a hole from the valence band to the lower spin sublevel of the conduction band. The only possible state, other than a magnetoplasmaron, which can be formed by a spin-cyclotron exciton and an e–h-pair, is a four-particle state — an exciton–magnetoplasmon molecule. This state is formed at high photoexcitation densities, when the probability of finding a photoexcited electron and a photoexcited hole simultaneously near a spin-cyclotron exciton increases.

The formation of an exciton–magnetoplasmon molecule can be described as follows. In the initial state, a biexciton exists consisting of a 'valence' p-type magnetoexciton and a purely electronic spin-cyclotron exciton. Then, a valence hole passes to the conduction band with the conservation of the inner quantum numbers of the exciton, and an exciton–

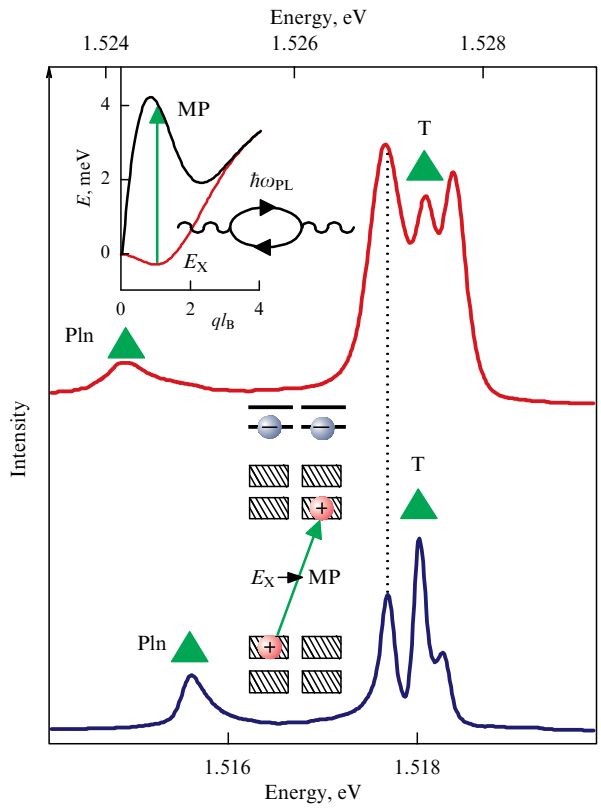

Figure 16. (Color online.) PL spectra for a narrow (17 nm, red curve, energy scale at the top) and a broad (35 nm, blue curve, energy scale at the bottom) QW. The energies of one-particle transitions in the σ^- polarization are made coincident. At the center the two-particle optical transition considered theoretically is shown. At the top left the Coulomb energies of two-particle excitations are shown calculated by disregarding second-order corrections for a spin-cyclotron exciton E_{X} (red curve) and a magnetoplasmon MP (black curve).

magnetoplasmon molecule is formed. The corresponding recombination line is shifted to lower energies due to the presence of plasmon oscillations in the final state. Two electrons in the magnetoexciton–magnetoplasmon molecule, unlike a magnetoplasmaron, can occupy one of the empty states (Fermi holes) at the zero Landau level. The unexpected result is that the contribution of the energy of plasma oscillations doubles (within the experimental accuracy) compared to plasmon contribution to the magnetoplasmaron energy, although two electrons and only one hole at the zero electronic Landau level are involved in plasma oscillations.

Thus, the PL spectra of 2D ESs have been studied in the presence of spin-cyclotron excitons. The ultralong relaxation times of nonequilibrium spin-cyclotron excitons in a quantizing magnetic field makes possible the existence of three- and four-particle complexes related to collective plasma oscillations of 2D ESs. The stability of these states (a two-hole magnetoplasmaron and a magnetoexciton-magnetoplasmon molecule) has been demonstrated. The existence of a stable magnetoexciton–magnetoplasmon molecule was not theoretically discussed earlier. Therefore, it is necessary to develop theoretical concepts for the quantitative description of experimental data. The further development of experimental studies comprises the investigation of photoinduced PL spectra in the presence of a dense (10^{10} cm^{-2}) ensemble of spin-cyclotron excitons.

8. Photoluminescence and the nondissipative spreading of a condensate of two-dimensional fermions and related spin excitations over macroscopically large distances. Detection methods

Despite the fact that the maximum fraction of spin-cyclotron excitons in a dense ensemble of 2D electrons in our experiments does not exceed 10% of the total number of electronic states at one spin Landau sublevel [32], all the oscillator strength of the photoinduced PL transfers to nonequilibrium recombination channels near a spin-cyclotron exciton (Figs 17 and 18). Note that an increase in the oscillator strength is observed in the region of the temperature curve where the number of nonequilibrium excitons in the photoexcitation spot does not increase but, on the contrary, decreases. Based on this quite unexpected observation, we can conclude that a phase transition occurs in the nonequilibrium electron system in which all the electrons at the upper spin sublevel of the zero Landau level not directly belonging to a spin-cyclotron exciton are nevertheless involved in a magnetofermion condensate, which is not only superabsorbing, but also superradiating.

Since superradiation is due to electrons under the Fermi level of the electron system, we can assume that during the formation of a nonequilibrium ensemble of spin-cyclotron excitons the excited electrons above the Fermi level are paired with electrons with the opposite spin below the Fermi level, modifying the electron vacuum. Correspondingly, the assumption about the invariability of the vacuum state to explain the coherent response of an ensemble of excitons to an external electromagnetic field is only a reasonable approximation describing the superabsorption effect, whereas a complete theory of the observed phase transition taking into account the superradiation effect has yet to be constructed. Also, it is necessary to find out whether this phase transition is an example of a topological BKT phase transition or we are dealing with a fundamentally new physical phenomenon.

Earlier, the unexpected behavior of the relaxation time of triplet excitons in the low-temperature region $T < 1$ K was reported where a new condensed phase appeared. In this region, the measured temperature dependence of the relaxation time is nonmonotonic (Fig. 12b). As temperature is decreased, this time begins to decrease strongly in the region where a new condensed phase appears. Such a behavior in no way can be related to the relaxation processes of magnetoexcitons, but rather indicates the 'nondiffusion' nature of the condensate spreading from the photoexcitation spot where the condensate is produced. The driving force producing the condensate spreading from the photoexcitation region to the boundary region with the unexcited 2D electron gas may be a large density gradient at the appearing interface. The hypothesis about the probable 'superdiffusion' spreading of the magnetofermion condensate over macroscopically large distances can be experimentally verified. To solve this

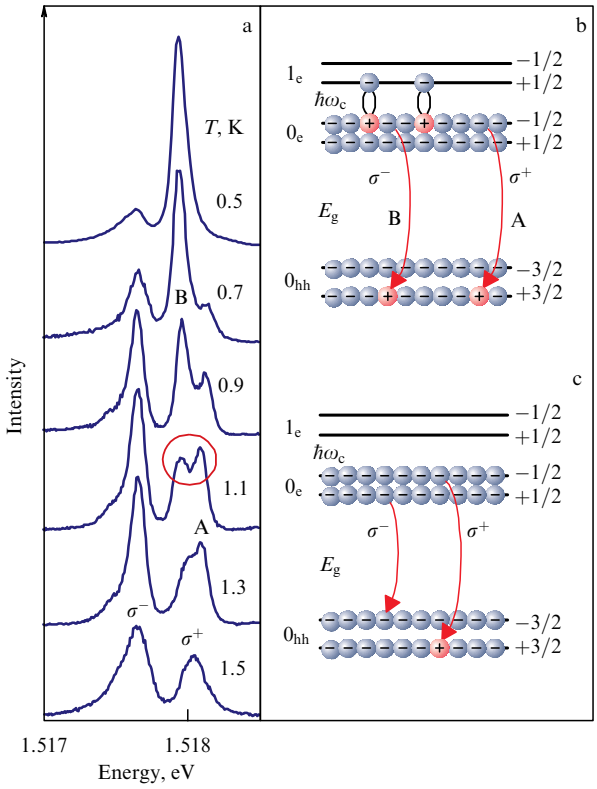

Figure 17. (a) PL spectra corresponding to the radiative recombination of electrons of the zero Landau level in the conduction band with heavy holes of the zero Landau level in the valence band measured in the temperature interval 1.5–0.5 K at the fixed pump $P = 32$ mW cm^{-2}. (b) Possible optical transitions in two polarizations in the equilibrium electronic system.

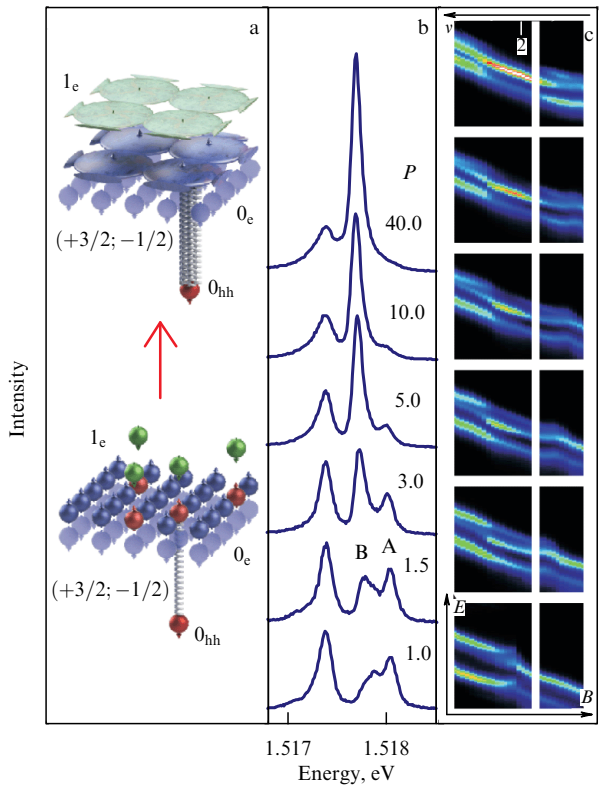

Figure 18. (a) Modification of the nonequilibrium electron density during formation of a condensate. (b) Evolution of the PL spectra of the condensate at the fixed temperature $T = 0.5$ K with various pumps under a magnetic field sweep (the condensate existence region lies in the range of electron filling factors $\nu \approx 2.00 \pm 0.15$). (c) PL spectra corresponding to the radiative relaxation of electrons of the zero Landau level in the conduction band with heavy holes of the zero Landau level in the valence band measured at the fixed temperature $T = 0.5$ K and different pumps P (mW cm^{-2}). The positions of maxima of electronic transitions from the lower spin Landau sublevel are reduced to the same energy.

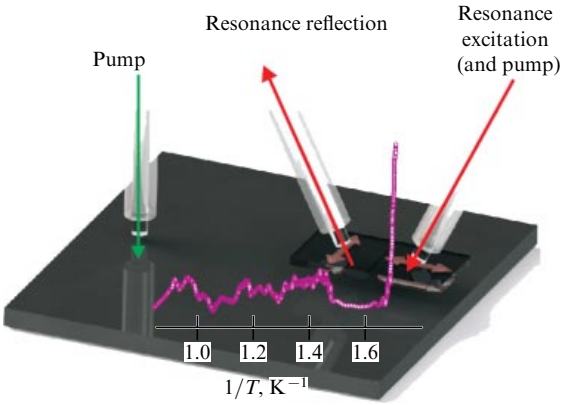

Figure 19. Diagram of PRR experiments with separated pump and probe regions. The standard PRR measurement setup is shown on the right. An additional pump fiber 400 μm in diameter is shown on the left. The inset shows the temperature dependence of the PRR signal detected at a distance of ≈ 2 mm from the excitation spot produced directly under the pump fiber.

problem, we developed and applied two independent methods. Each of them used the spatial separation of the excitation and detection regions of the spreading condensate.

In the first method, optical fibers for excitation and direct detection of spin-cyclotron excitons in a condensed phase by the PRR method were spatially separated [99]. Figure 19 illustrates the experimental setup and the result of the experimental observation of the condensate spreading over macroscopically large distances from the local direct optical excitation region.

A sufficiently dense ensemble of spin-cyclotron excitons in the 2D fermion electron system was excited by laser light via the additional third fiber shown in the left part of Fig. 19. Magnetoexcitons are excited in a laser spot about 0.4 mm in diameter located directly under the fiber. Two other fibers located at a distance of 2 mm from the first fiber (in the right part of Fig. 19), i.e., sufficiently far from the condensate photocreation region, are used for PRR measurements related to Fermi holes (electron vacancies) in triplet magnetoexcitons created under the remote (left) fiber.[8] When the temperature of the system under study is relatively high, $T > 1$ K, the PRR signal related to Fermi holes belonging to triplet magnetoexcitons is minor, even at high photoexcitation densities and lost in the noise caused by the residual light scattering in a cryosystem. However, as temperature is decreased at the same fixed optical pumping in the region $T \leqslant 0.75$ K, the giant threshold PRR increase is observed. This observation, consistent with the phase diagram presented in Fig. 13, proves that a considerable part of photoexcited spin-cyclotron excitons condensed in a 2D fermion electron system spreads nondiffusively from the excitation region over macroscopically large distances.

As was pointed out, the decrease in the relaxation time of these excitations measured by time-resolved PRR proves to be false in reality. We are not dealing with the acceleration of relaxation of spin-cyclotron excitons but with their 'escape'

[8] Later, the condensate spreading picture was visualized upon photoexcitation in a spot 20 μm in diameter and PRR detection with a broad beam from the adjacent region ⩾ 200 μm. The condensate spreading length in these experiments exceeded the detection region size restricted by the aperture of the optical system used [102].

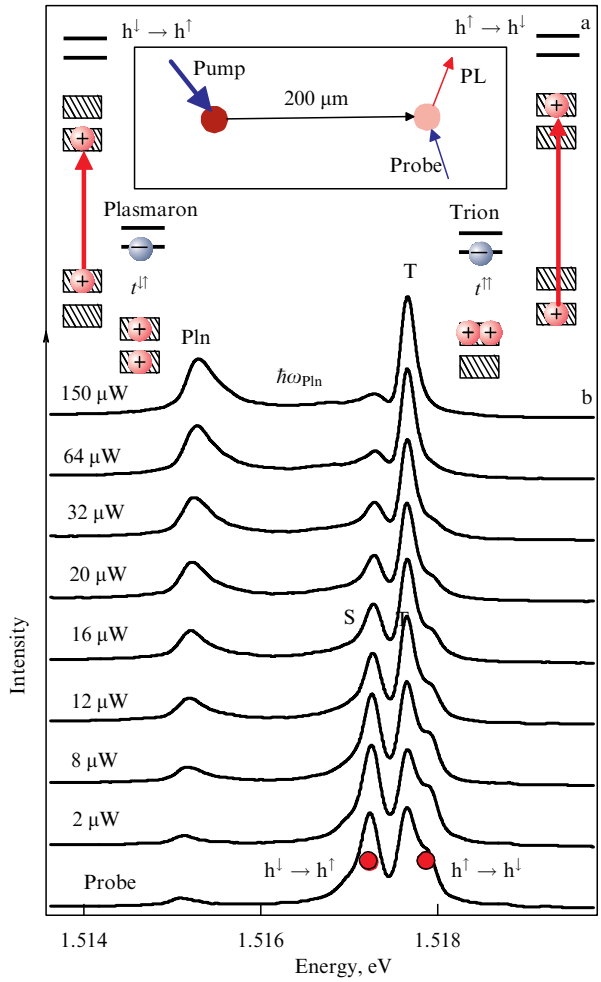

Figure 20. (a) Schematic diagrams of experiment and single-particle transitions in two polarizations of the emitted photon. Shown are two possible final three-particle states of the recombination process in the presence of spin-cyclotron excitons, called a trion and a plasmaron. (b) Evolution of PL line intensities for different recombination channels of a photoexcited hole in the probe region at the increase of the excitation power in the pump region.

from the excitation spot, which was shown in [103] from the PL study of three-particle complexes: magnetotrions and magnetoplasmarons. To verify this assumption, samples with 2D ES were placed in an evacuated insert with liquid ^{3}He having an optical window for input/output of radiation, which, in turn, was placed into a ^{4}He cryostat with a superconducting solenoid. The beam of an exciting tunable laser was split into pump and probe beams. Laser beams were focused by lenses inside the ^{3}He cryostat on the surface of a sample into two spatially separated round spots 20 μm in diameter each. The distance between the centers of the pump and probe spots was 200 μm (Fig. 20a). The pump power density was varied within two orders of magnitude from 2 to 200 μW, while the probe beam power was maintained constant and equal to 3 μW.

For weak pump levels below 6 μW, the shape of the spectrum and recombination signal from the probe region did not change, indicating that the ensemble of spin magnetoexcitons from the excitation region does not affect states in the probe regions (Fig. 20b). However, as the pump power was further increased, the PL signal shape in the probe region changed, namely, the intensity of lines related to optical

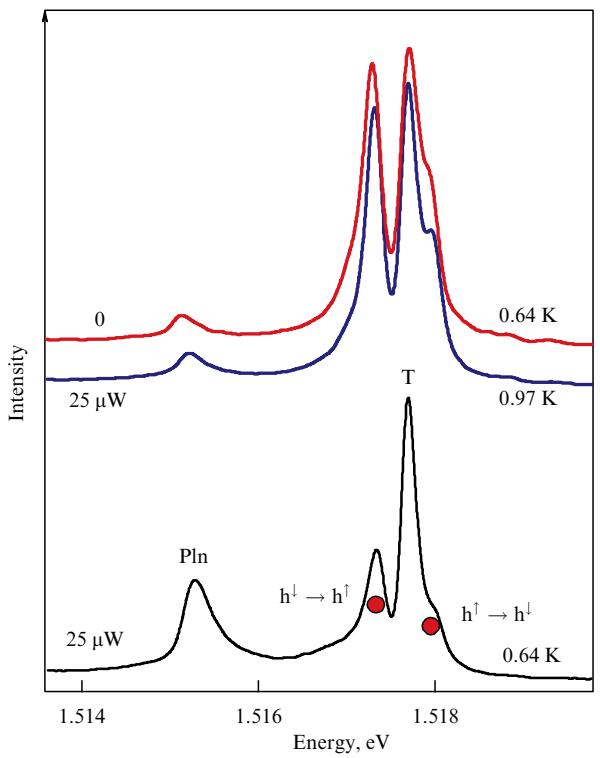

Figure 21. (Color online.) PL spectra from the probe region obtained upon fixed pumping $P = 25$ μW in the excitation region at different temperatures below and above the transition point to the condensed state of a nonequilibrium ensemble of spin-cyclotron excitons. For comparison, the low-temperature PL spectrum is shown in the absence of laser pumping in the excitation region (red curve).

transitions in three-particle complexes (magnetotrions and magnetoplasmarons) increased [100]. Thus, optical transitions involving three-particle complexes are 'signal markers' indicating the appearance of spin-cyclotron excitons in the probe region produced in the excitation region.

When the critical pump power (about 6 μW) in the excitation region is exceeded, spin-cyclotron excitons begin to arrive at the probe spot, their propagation distance reaching giant values (up to 200 μm) restricted in the experiment only by the region size determined by the aperture of the optical system. The exciton transport can be stopped by increasing the temperature of the electronic system (Fig. 21). As the temperature increases by 0.3 K, PL spectra from the probe region take the same shape as in the absence of excitation in the pump region, although the pump itself remains invariable. This means that the transport of spin-cyclotron excitons and, respectively, the spatial spin transfer from the excitation region completely cease. This is consistent with exciton lifetime measurements, which revealed that the exciton lifetime in the excitation spot decreased in the same temperature range where the exciton transport from the pump spot was observed in this experiment.

9. Promising areas of further studies: the excitation and relaxation of spin-texture and spin Laughlin liquids

A number of problems are still unsolved and poorly studied in the field of investigations discussed in this review. First of all, this concerns a theoretical description of the magnetofermion phase itself in a quantum Hall insulator. Experimental studies of the spatiotemporal coherence of a condensed phase (first- and second-order correlators) and of the propagation velocity of spin excitations in 2D electron gas quantized in a magnetic field could shed light on the microscopic structure and thereby the description of the order parameter of a magnetofermion condensate.

The observation of a condensate spreading with the integer spin transfer over macroscopically large distances opens up the unique possibility for spin control with the help of external actions (gate voltage, temperature, and an optical pump) for creating a spin transistor. Along with this, noticeable progress in describing spin relaxation in a quantum Hall ferromagnet opens up possibilities for solving more complicated problems such as describing spin relaxation for small deviations of the electron filling factor from odd integer values and in fractional Laughlin states. Problems complicating the theoretical description of the spin relaxation in these two cases appear for different reasons. In the case of small deviations of ν from odd integer values, the structure of the ground state of the electronic system is unknown, whereas the spectrum of spin excitations is experimentally measured. In the case of Laughlin liquids [104], the ground-state wave function is well known; however, the spectrum of collective spin excitations is unknown.

It is accepted that, when the filling factor deviates from unity to a larger (smaller) value, the electron spins form vortex-like topological spin textures called skyrmions (anti-skyrmions). Skyrmions (anti-skyrmions) appear due to competition between the Zeeman and exchange energies. In high-mobility $GaAs/Al_xGa_{1-x}As$ semiconductor 2D systems, the Zeeman energy is rather considerable, while the number of inverted spins in a skyrmion does not exceed four. In this connection, the theory of spin-texture particles with several inverted spins, which are the quantum generalization of classical skyrmions, was developed.

It was assumed that spin-textured quasi-particles in the ground state form a crystal lattice [105]. The first experimental data suggesting the formation of a skyrmion crystal lattice were obtained in 3D MnSi ferromagnetic films and similar compounds [106]. However, no conclusive evidence was presented about the existence of a skyrmion crystal in a quantum Hall ferromagnet with charged defects formed due to either a deficiency or excess of the electronic density. Moreover, the entire theory of spin-texture quasi-particles in 2D ESs was subject to doubt. The spin depolarization of the electron system in the vicinity of the unity filling factor proved to be completely reproducible for filling factors in the vicinity of $\nu = 3$ (Fig. 22), where the existence of spin-texture quasi-particles is doubtful, even for the zero Zeeman energy [107]. The effective number of inverted spins determined from new optical spin-polarization studies in 2D systems is not consistent with previous experimental data [74]. Nor does this number agree with theoretical values, despite the fact that it should be certainly determined by the ratio of the Zeeman and exchange energies. Finally, it was shown that physical objects similar to spin-texture quasi-particles exist in the limit of the zero number of inverted spins [88, 89].

Based on ILS observations of spin-excitation spectra, it was assumed that the ground state of a quantum Hall ferromagnet with charge defects caused by a deficiency or excess of electronic density is a spin-texture liquid. In the excitation spectrum of the liquid, new gap branches appear related to the collective precession of the electron spin in the

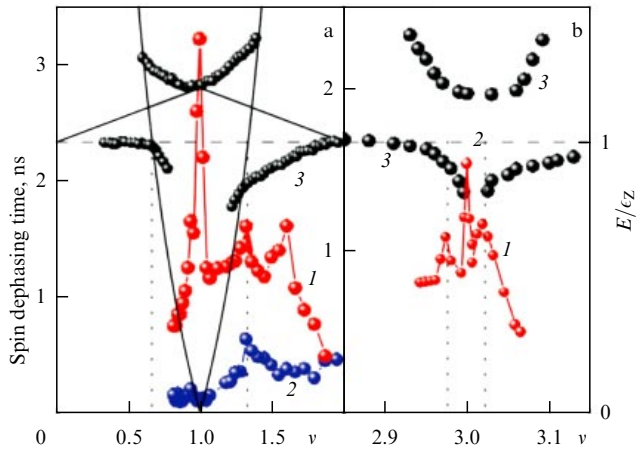

Figure 22. (Color online.) Decay time of a long-lived Kerr signal (left vertical axis) recorded in the spectral position corresponding to lower-energy optical transition (*1* — red) and to the higher-energy optical transition (*2* — blue) as a function of the filling factor: (a) near $\nu = 1$ (the total magnetic field is $B = 4.50$ T, sample A) and (b) $\nu = 3$ ($B = 4.65$ T, sample B). Samples are described in Section 4. Solid curves show theoretical dependences for 'cyclotron' spin excitations in a spin-texture liquid and the energy of a spin magnetoexciton obtained in the Hartree–Fock approximation [85]. The dashed line shows the Larmor energy. Dotted lines are drawn for convenience. Black dots show the energies of collective spin excitations (right vertical axis) measured in [88, 89].

effective magnetic field produced by spin textures. New excitation branches behave similarly to cyclotron excitations, albeit, not in the external magnetic field but in some fictitious magnetic field proportional to the density of spin-texture quasi-particles. Correspondingly, the 'effective mass' of collective spin excitations is determined by the polarization degree of the electronic system and the exchange interaction strength [88, 89].

The authors of the review performed spin-relaxation experiments for small deviations of the filling factor from odd integer values. We found a nonmonotonic dependence of the spin relaxation time on the filling factor for ν close to filling factors corresponding to quantum Hall ferromagnetic states. The nonmonotonic dependence is explained by the fact that the spin-excitation energy of spin-texture liquids can be either higher or lower than the Zeeman energy. This leads to the appearance and disappearance of additional relaxation channels of spin excitons having the Zeeman energy. The spin excitations of spin-texture liquids are related to transitions between the 'effective Landau levels' of electron spins caused by the Berry phase [108], which is acquired during the precession of the electron spin around spin textures. For odd integer filling factors, the energy of these excitations is exactly zero, because spin textures are absent. In turn, the energy increases with increasing density of spin textures and begins to exceed the Zeeman energy at some density value. According to theoretical estimates [109], this electron energy at the Landau level is proportional to the spin texture density and the exchange energy

$$\hbar\omega_c' = \frac{1}{2} E_x \frac{1-\nu}{\nu} ,$$

where E_x is the exchange energy [109]. Experimental spin-relaxation data agree qualitatively with the results of Ref. [109]; however, the existing theory ignores the strong interaction of different spin-excitation branches, which was found experimentally. It seems that, to obtain quantitative agreement between experiments and theory, additional experimental efforts are required, and the theory of spin-textured liquids should be further developed.

Direct measurements of the spin relaxation and an explanation for relaxation mechanisms are even more important for Laughlin uncompressible liquids. Laughlin liquids [104] formed in the case of the fractional quantum Hall effect have been discussed in numerous publications. The attention of the scientific community devoted to this topic can be compared only to superconductivity and superfluidity phenomena. However, unlike the theory of these widely known physical phenomena, so far no consistent microscopic (nonphenomenological) theory exists which could be used to construct the ground state, even for the most known and well-studied Laughlin state with $\nu = 1/3$. The situation with other fractional states proves to be even less predictable. The microscopic theory of composite fermions [110], in the opinion of its authors themselves, can be applied only in the vicinity of the filling factor $\nu = 1/2$ and cannot be extended to Laughlin states, whereas phenomenological theories of type [111] use a number of assumptions which seem to be not entirely justified.

For example, it was recently shown that the formation of Laughlin liquids does not require the smallness of the interparticle Coulomb interaction energy compared to the cyclotron quantization energy. Laughlin states are observed not only in high-mobility $GaAs/Al_xGa_{1-x}As$ QWs and heterojunctions for which this assumption is well satisfied, but also in new 2D heterostructures such as heterojunctions in ZnO/MgZnO oxides [112]. Despite substantially different characteristics of these objects (permittivity and mass of carriers), the properties of Laughlin states prove to be universal and weakly sensitive to the specific features of the systems studied. Moreover, in the ZnO/MgZnO system under conditions of the fractional quantum Hall effect, we can easily come to the smallness of the ratio of the cyclotron quantization energy to the interparticle Coulomb interaction energy. Nevertheless, all the main Laughlin states are experimentally observed. The exclusion is fractional states with even denominators, which are, however, usually related either to the ground-state anisotropy or to the nontrivial interparticle ordering.

What hinders progress in the study of Laughlin states? The answer becomes obvious if we consider experimental methods used for solving this problem.

The main method for studying Laughlin liquids is magnetotransport, which is associated with a number of symmetry restrictions that actually prohibit the use of other experimental techniques for these purposes. For example, the Kohn and Larmor theorems restrict the applicability of such powerful experimental methods as the cyclotron resonance (CR) and electron spin resonance (ESR). Infrared absorption spectroscopy, in combination with the formation of a grating of surface acoustic waves (SAWs), can alleviate symmetry restrictions. However, such an approach requires considerable methodological efforts, which in turn restricts the applicability of CR and ESR in modulated SAW structures [85]. The potential of using optical methods such as PL, optical absorption, and photoexcitation is also restricted. For optical transitions with zero transfer momenta, a so-called hidden symmetry exists [113], which makes optical spectra insensitive to variations in the ground state of the 2D system in the ultra-quantum limit.

The main requirements for a system with hidden symmetry are:

(1) The presence of charge symmetry at which the interaction potentials of electrons and holes have equal values ($V_{ee} = V_{hh} = -V_{eh}$, where subscripts e and h refer to electrons in the conduction band and holes in the valence band, respectively);

(2) the electron system must be in the quantum limit $\nu \leqslant 2$;

(3) the mixing of Landau levels is disregarded.

The first condition is violated in wide QWs with one-sided doping and in two-layer systems when the electron layer is separated from the layer of photoexcited holes and, as a result, the envelopes of the electron and hole wave functions in the growth direction of heterostructures are displaced in the coordinate space with respect to each other. Even in this case, the energy of optical transitions weakly depends on the change in the ground state of the electron system [114].

As for narrow $GaAs/Al_xGa_{1-x}As$ QWs in which the envelope of wave functions of charge carriers is specified not by the electric field of doping impurities but by the quantizing potential, condition (1) for them can be assumed fulfilled. Less obvious is the fulfillment of condition 1 in the QW plane because of the complicated structure of Landau levels in the GaAs valence band.

Condition 2 is a formal statement concerning the carrier concentration, which can, in fact, always be fulfilled.

The situation with condition 3 is not so unambiguous. Theoretical models describing optical transitions in the ultraquantum limit usually take into account the energy contributions of the first-order smallness in the Coulomb/cyclotron energy ratio. Such an approach assumes that the higher-lying Landau levels are ignored in calculations of optical transition energies. Electron correlations related to the formation of Laughlin liquids in the ground state are included in the single-mode approximation, which also ignores the higher-lying Landau levels, i.e., condition 3 is a priori assumed fulfilled [115–117]. Thus, condition 3 is usually ignored in theoretical estimates of the optical spectra of 2D systems; however, in experimentally implementable systems this disregard is obviously unjustified, especially in light of experiments with ZnO/MgZnO heterostructures.

Despite modern theoretical concepts, the authors of the review have managed for the first time to distinguish in the resonance optical reflection spectra of 2D ES a line related to excitation of a Laughlin liquid with $\nu = 1/3$ (Fig. 23). The line is observed in the symmetric electronic system, where condition 1 is partially satisfied and condition 2 is completely fulfilled, for the zero transfer momentum in a translation-invariant system (reflection). The new line is shifted to the blue by the energy, which is interpreted as the Coulomb gap required for creating a neutral spin defect in the uncompressible Laughlin liquid.

The observation of an individual line from the Laughlin liquid in the resonance reflection spectrum of the 2D ES is important not only from the fundamental scientific but also from the methodological point of view. This makes possible the optical probing of uncompressible liquids in translation-symmetric 2D systems (which has so far been impossible using optical, CR, and ESR methods) and time-resolved optical studying of the relaxation dynamics of spin excitations in Laughlin uncompressible liquids, as in [83].

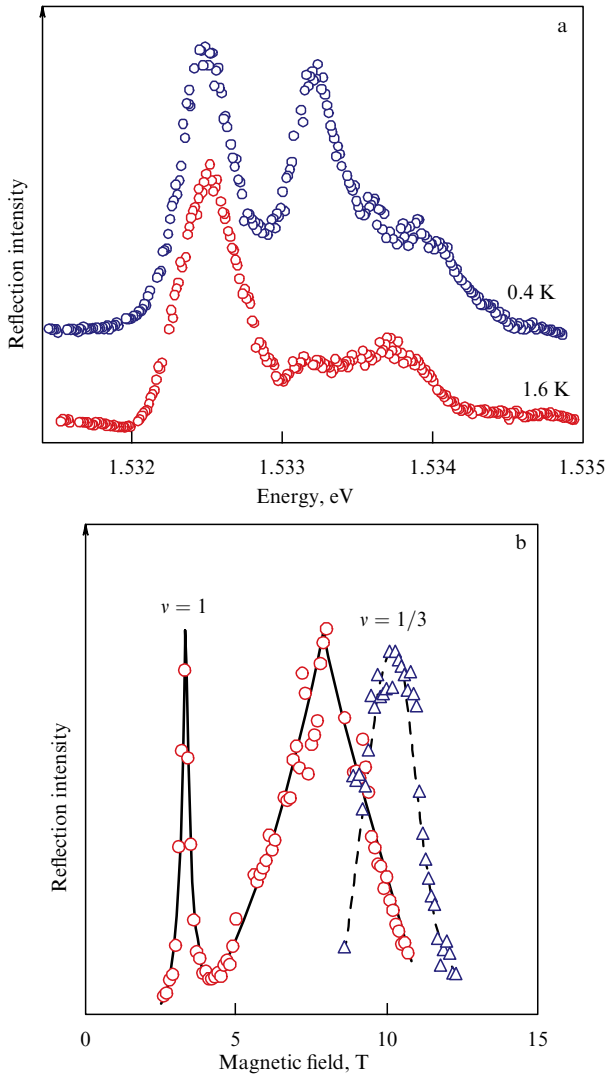

Figure 23. (Color online.) Resonance reflection of light for optical transitions from the zero Landau level in the valence band to the upper spin sublevel of the zero Landau level in the conduction band. (a) Reflection spectrum in the magnetic field region where a new low-temperature resonance reflection line from a Laughlin liquid is observed for $\nu = 1/3$. (b) Magnetic-field dependences of spectral line intensities in the regions of magnetic-field strengths at which the Laughlin liquid is formed (blue triangles) or is not formed (red circles). The curves are drawn for the convenience of readers.

Addition in proofs. During the review preparation for publication, noticeable progress appeared in the understanding of the physics of 'dark' triplet magnetoexcitons and a magnetofermion condensate. The study of the PRR signal decay kinetics excited by a pump pulse with the simultaneous control of the PL spectrum and analysis of PL spectra in the case of the spatial separation of pump and probe pulses was used in the method for constructing the distribution of spin magnetoexcitons over generalized momenta [118–121]. It was found that only excitons with momenta $q \approx 1/l_B$ spread over macroscopic distances. Because the laws of conservation of energy and momentum cannot be simultaneously satisfied, complete thermalization does not occur in an ensemble of dark magnetoexcitons. Relaxation to the lowest energy state proceeds due to two-exciton processes, which become noticeable only when some critical exciton density is reached. Because of ultralong thermalization times, the ensemble of dark magnetoexcitons is substantially nonequilibrium and consists of two components. One of them is above-condensate

magnetoexcitons with generalized momenta $q \approx 0$ and the other is magnetoexcitons with momenta $q \approx 1/l_B$ involved in the formation of a magnetofermion condensate and transport over macroscopic distances. Thus, a photoexcited system of spin magnetoexcitons substantially differs from a system of indirect excitons in the momentum space in 3D semiconductors (Ge, Si), where long-lived excitons are thermalized during their lifetime [122]. A closer example of a nonequilibrium Bose system is parametrically pumped high-temperature Bose–Einstein magnon condensates in yttrium-ferrum garnet films [47]. Pulsed photoexcitation experiments show in [119] that the spreading rate of a magnetofermion condensate is no less than 25 m s^{-1}, which is not greatly different from these rates in a magnon condensate [123]. Progress in the theoretical description of the optical properties of spin excitons in a Hall dielectric is described in [124].

Acknowledgments
The authors thank M A Khit'ko for help in the preparation of the review text. The study was supported by the Russian Science Foundation (grant no. 16-12-10075).

References

1. Žutić I, Fabian J, Das Sarma S *Rev. Mod. Phys.* **76** 323 (2004)
2. Cornelissen L J et al. *Nature Phys.* **11** 1022 (2015)
3. Büttner F et al. *Nature Phys.* **11** 225 (2015)
4. Datta S, Das B *Appl. Phys. Lett.* **56** 665 (1990)
5. Kiss A, Szolnoki L, Simon F *Sci. Rep.* **6** 22706 (2016)
6. Boross P et al. *Sci. Rep.* **3** 3233 (2013)
7. Alphenaar B W, Müller H O, Tsukagoshi K *Phys. Rev. Lett.* **81** 5628 (1998)
8. Fukuoka D et al. *Phys. Rev. B* **78** 041304(R) (2008)
9. Fukuoka D et al. *Phys. Rev. Lett.* **105** 126802 (2010)
10. Nefyodov Yu A et al. *JETP Lett.* **91** 357 (2010); *Pis'ma Zh. Eksp. Teor. Fiz.* **91** 385 (2010)
11. Frenkel D M *Phys. Rev. B* **43** 14228 (1991)
12. Dikman S M, Iordanskii S V *JETP* **83** 128 (1996); *Pis'ma Zh. Eksp. Teor. Fiz.* **110** 238 (1996)
13. Dickmann S *Phys. Rev. Lett.* **93** 206804 (2004)
14. Dickmann S, Ziman T *Phys. Rev. B* **85** 045318 (2012)
15. Dickmann S *Phys. Rev. Lett.* **110** 166801 (2013)
16. Bisti V E et al. *Phys. Usp.* **58** 315 (2015); *Usp. Fiz. Nauk* **185** 337 (2015)
17. Keldysh L V, Kozlov A N *JETP Lett.* **5** 190 (1967); *Pis'ma Zh. Eksp. Teor. Fiz.* **5** 238 (1967)
18. Keldysh L V, Kozlov A N *Sov. Phys. JETP* **27** 521 (1968); *Pis'ma Zh. Eksp. Teor. Fiz.* **54** 978 (1968)
19. Keldysh L V "Kogerentnye sostoyaniya eksitonov" ("Coherent exciton states"), in *Problemy Teoreticheskoi Fiziki. Pamyati Igorya Evgen'evicha Tamma* (Problems of Theoretical Physics. To the Memory of Igor Evgen'evich Tamm) (Ed. V I Ritus) (Moscow: Nauka, 1972) p. 433
20. Keldysh L V *Phys. Usp.* **60** 1180 (2017); *Usp. Fiz. Nauk* **187** 1273 (2017)
21. Dzyubenko A B, Lozovik Yu E *Sov. Phys. Solid State* **25** 874 (1983); *Fiz. Tverd. Tela* **25** 1519 (1983)
22. Dzyubenko A B, Lozovik Yu E *Sov. Phys. Solid State* **26** 938 (1984); *Fiz. Tverd. Tela* **26** 1540 (1984)
23. Gor'kov L P, Dzyaloshinskii I E *Sov. Phys. JETP* **26** 449 (1968); *Zh. Eksp. Teor. Fiz.* **53** 717 (1967)
24. Laikhtman B *J. Phys. Condens. Matter* **19** 295214 (2007)
25. Dzyubenko A B, Lozovik Y E *J. Phys. A* **24** 415 (1991)
26. Lifshitz E M, Pitaevskii L P *Statistical Physics* Pt. 2 *Theory of the Condensed State* (Oxford: Butterworth-Heinemann, 1980); Translated from Russian: *Statisticheskaya Fizika* Ch. 2 *Teoriya Kondensirovannogo Sostoyaniya* (Moscow: Fizmatlit, 2004)
27. Kohn W *Phys. Rev.* **123** 1242 (1961)
28. Bychkov Yu A, Iordanskii S V, Eliashberg G M *JETP Lett.* **33** 143 (1981); *Pis'ma Zh. Eksp. Teor. Fiz.* **33** 152 (1981)
29. Kallin C, Halperin B I *Phys. Rev. B* **30** 5655 (1984)
30. Kulik L V et al. *Phys. Rev. B* **72** 073304 (2005)
31. Dickmann S, Kukushkin I V *Phys. Rev. B* **71** 241310(R) (2005)
32. Kulik L V et al. *Sci. Rep.* **5** 10354 (2015)
33. Lerner I V, Lozovik Yu E *Sov. Phys. JETP* **53** 763 (1981); *Zh. Eksp. Teor. Fiz.* **80** 1488 (1981)
34. Hohenberg P C *Phys. Rev.* **158** 383 (1967)
35. Mermin N D, Wagner H *Phys. Rev. Lett.* **17** 1133 (1966)
36. Berezinskii V L *Sov. Phys. JETP* **32** 493 (1970); *Zh. Eksp. Teor. Fiz.* **59** 907 (1970)
37. Berezinskii V L *Sov. Phys. JETP* **34** 610 (1971); *Zh. Eksp. Teor. Fiz.* **61** 1144 (1971)
38. Kosterlitz J M, Thouless D J *J. Phys. C* **6** 1181 (1973)
39. Bishop D J, Reppy J D *Phys. Rev. Lett.* **40** 1727 (1978)
40. Bishop D J, Reppy J D *Phys. Rev. B* **22** 5171 (1980)
41. van der Zant H S J, Rijken H A, Mooij J E *J. Low Temp. Phys.* **82** 67 (1991)
42. Hadzibabic Z et al. *Nature* **441** 1118 (2006)
43. Cladé P et al. *Phys. Rev. Lett.* **102** 170401 (2009)
44. Roumpos G et al. *Nature Phys.* **7** 129 (2011)
45. Eisenstein J P, MacDonald A H *Nature* **432** 691 (2004)
46. Kasprzak J et al. *Nature* **443** 409 (2006)
47. Demokritov S O et al. *Nature* **443** 430 (2006)
48. Anderson M H et al. *Science* **269** 198 (1995)
49. Davis K B et al. *Phys. Rev. Lett.* **75** 3969 (1995)
50. Moskalenko S A et al. *Phys. Solid State* **55** 1563 (2013); *Fiz. Tverd. Tela* **55** 1457 (2013)
51. Lozovik Yu E, Yudson V I *Sov. Phys. JETP* **44** 389 (1976); *Zh. Eksp. Teor. Fiz.* **71** 738 (1976)
52. Timofeev V B, Gorbunov A V, Demin D A *Low Temp. Phys.* **37** 179 (2011); *Fiz. Nizk. Temp.* **37** 229 (2011)
53. Gorbunov A V, Timofeev V B *JETP Lett.* **37** 138 (2012); *Pis'ma Zh. Eksp. Teor. Fiz.* **96** 145 (2012)
54. Osheroff D D, Richardson R C, Lee D M *Phys. Rev. Lett.* **28** 885 (1972)
55. Regal C A, Greiner M, Jin D S *Phys. Rev. Lett.* **92** 040403 (2004)
56. Larionov A V et al. *Phys. Rev. B* **92** 165417 (2015)
57. Lord Rayleigh F R S *Philos. Mag. 5* **47** 375 (1899)
58. Bohren C F, Huffman D R *Absorption and Scattering of Light by Small Particles* (New York: John Wiley, 1983)
59. Ginzburg V L, Levanyuk A P, Sobyanin A A *Phys. Rep.* **57** 151 (1980)
60. Hegarty J et al. *Phys. Rev. Lett.* **49** 930 (1982)
61. Haacke S *Rep. Prog. Phys.* **64** 737 (2001)
62. Sibel'din N N, Skorikov M L, Tsvetkov V A *JETP Lett.* **76** 628 (2002); *Pis'ma Zh. Eksp. Teor. Fiz.* **76** 732 (2002)
63. Luin S et al. *Phys. Rev. Lett.* **97** 216802 (2006)
64. Rhone T D et al. *Phys. Rev. Lett.* **106** 196805 (2011)
65. Bellani V et al. *Phys. Rev. B* **83** 193307 (2011)
66. Kulik L V et al. *Phys. Rev. B* **85** 113403 (2012)
67. Belitsky V I et al. *Phys. Rev. B* **52** 16665 (1995)
68. Garro N et al. *Phys. Rev. B* **55** 13752 (1997)
69. Ando T, Fowler A B, Stern F *Rev. Mod. Phys.* **54** 437 (1982)
70. Bisti V E et al. *JETP Lett.* **98** 778 (2013); *Pis'ma Zh. Eksp. Teor. Fiz.* **98** 877 (2013)
71. Manfra M J et al. *Phys. Rev. B* **54** 17327(R) (1996)
72. Groshaus J G et al. *Phys. Rev. Lett.* **98** 156803 (2007)
73. Aifer E H, Goldberg B B, Broido D A *Phys. Rev. Lett.* **76** 680 (1996)
74. Plochocka P et al. *Phys. Rev. Lett.* **102** 126806 (2009)
75. Kukushkin I V, v. Klitzing K, Eberl K *Phys. Rev. B* **55** 10607 (1997)
76. Dikman S M, Iordanskii S V *JETP Lett.* **63** 50 (1996); *Pis'ma Zh. Eksp. Teor. Fiz.* **63** 43 (1996)
77. Dikman S M, Iordanskii S V *JETP Lett.* **70** 543 (1999); *Pis'ma Zh. Eksp. Teor. Fiz.* **70** 531 (1999)
78. Dickmann S *JETP Lett.* **78** 452 (2003); *Pis'ma Zh. Eksp. Teor. Fiz.* **78** 921 (2003)
79. Dickmann S, Artyukhin S L *JETP Lett.* **89** 133 (2009); *Pis'ma Zh. Eksp. Teor. Fiz.* **89** 153 (2009)
80. Dickmann S *JETP Lett.* **93** 86 (2011); *Pis'ma Zh. Eksp. Teor. Fiz.* **93** 88 (2011)
81. Burkov A A, Balents L *Phys. Rev. B* **69** 245312 (2004)
82. Barrett S E et al. *Phys. Rev. Lett.* **74** 5112 (1995)
83. Zhuravlev A S et al. *Phys. Rev. B* **89** 161301(R) (2014)

84. Gallais Y et al. *Phys. Rev. Lett.* **100** 086806 (2008)
85. Kukushkin I V et al. *Science* **324** 1044 (2009); Supporting Online Material, https://science.sciencemag.org/content/suppl/2009/04/30/1171472.DC1
86. Landau L D, Lifshitz E M *Statistical Physics* Pt. 1 (Oxford: Butterworth-Heinemann, 1980); Translated from Russian: *Statisticheskaya Fizika* Ch. 1 (Moscow: Fizmatlit, 2005)
87. Larionov A V, Zhuravlev A S *JETP Lett.* **97** 137 (2013); *Pis'ma Zh. Eksp. Teor. Fiz.* **97** 156 (2013)
88. Drozdov I K et al. *Phys. Rev. Lett.* **104** 136804 (2010)
89. Kulik L V et al. *Phys. Rev. B* **87** 045316 (2013)
90. Landau L D, Lifshitz E M *Quantum Mechanics: Non-Relativistic Theory* (Oxford: Pergamon Press, 1977); Translated from Russian: *Kvantovaya Mekhanika: Nerelyativistskaya Teoriya* (Moscow: Fizmatlit, 2004)
91. Apel W, Bychkov Yu A *Phys. Rev. Lett.* **82** 3324 (1999)
92. Khaetskii A V *Phys. Rev. Lett.* **87** 049701 (2001)
93. Apel W, Bychkov Yu A *Phys. Rev. Lett.* **87** 049702 (2001)
94. Dickmann S, arXiv:1709.06811
95. Tycko R et al. *Science* **268** 1460 (1995)
96. Zhang Q et al. *Phys. Rev. Lett.* **113** 047601 (2014)
97. Blackwood E et al. *Phys. Rev. B* **50** 14246 (1994)
98. Bayer M et al. *Phys. Rev. Lett.* **82** 1748 (1999)
99. Kulik L V et al. *Nature Commun.* **7** 13499 (2016)
100. Zhuravlev A S et al. *Phys. Rev. Lett.* **117** 196802 (2016)
101. Dzyubenko A B, Sivachenko A Yu *Phys. Rev. Lett.* **84** 4429 (2000)
102. Kulik L V et al. *Sci. Rep.* **8** 10948 (2018)
103. Gorbunov A V et al. *JETP Lett.* **106** 682 (2017); *Pis'ma Zh. Eksp. Teor. Fiz.* **106** 651 (2017)
104. Laughlin R B *Phys. Rev. Lett.* **50** 1395 (1983)
105. Côté R et al. *Phys. Rev. Lett.* **78** 4825 (1997)
106. Mühlbauer S et al. *Science* **323** 915 (2009)
107. Cooper N R *Phys. Rev. B* **55** 1934(R) (1997)
108. Berry M V *Proc. R. Soc. Lond. A* **392** 45 (1984)
109. Rodriguez J P *Europhys. Lett.* **42** 197 (1998)
110. Halperin B I, Lee P A, Read N *Phys. Rev. B* **47** 7312 (1993)
111. Murthy G, Shankar R *Rev. Mod. Phys.* **75** 1101 (2003)
112. Tsukazaki A et al. *Nature Mater.* **9** 889 (2010)
113. Apalkov V M, Rashba E I *Phys. Rev. B* **46** 1628 (1992)
114. Byszewski M et al. *Nature Phys.* **2** 239 (2006)
115. Girvin S M, MacDonald A H, Platzman P M *Phys. Rev. Lett.* **54** 581 (1985)
116. Girvin S M, MacDonald A H, Platzman P M *Phys. Rev. B* **33** 2481 (1986)
117. Longo J P, Kallin C *Phys. Rev. B* **47** 4429 (1993)
118. Kuznetsov V A et al. *Phys. Rev. B* **98** 205303 (2018)
119. Kulik L V et al. *Appl. Phys. Lett.* **114** 062403 (2019)
120. Gorbunov A V et al. *Ann. Physik* **531** 1800443 (2019)
121. Zhuravlev A S et al. *JETP Lett.* **110** 284 (2019); *Pis'ma Zh. Eksp. Teor. Fiz.* **110** 260 (2019)
122. Sibeldin N N *Phys. Usp.* **60** 1147 (2017); *Usp. Fiz. Nauk* **187** 1236 (2017)
123. Sun C, Nattermann T, Pokrovsky V L *J. Phys. D* **50** 143002 (2017)
124. Dickmann S *Lithuanian J. Phys.* **59** 79 (2019)